Research article

JGS
Journal of the Geological Society

https://doi.org/10.1144/jgs2022-037 | Vol. 180 | 2022 | jgs2022-037

# Mid-crustal reactivation processes linked to frictional melting and deep void development during seismogenic slip: examples from the Lewisian Complex, NW Scotland

**K. Hardman[1], R. E. Holdsworth[1,2]*, L. Scott[1], E. Dempsey[3] and K. J. W. McCaffrey[1,2]**

[1] Department of Earth Sciences, Durham University, Durham DH1 3LE, UK
[2] Geospatial Research Ltd, Durham DH1 4EL, UK
[3] Department of Geography, Geology and Environment, University of Hull, Hull HU6 7RX, UK
REH, 0000-0002-3467-835X
* Correspondence: r.e.holdsworth@durham.ac.uk

**Abstract:** Exhumed examples of ancient fault voids formed during seismic slip at depths >10 km are well preserved in the Assynt Terrane of the Lewisian Complex, NW Scotland. They are interpreted to have formed during regional Mesoproterozoic (*c.* 1.55 Ga; 'Assyntian') strike-slip faulting. Deformation is characterized by sinistral reactivation of pre-existing NW–SE-trending features including intrusive contacts of (*c.* 2.4 Ga) mafic dykes and Paleoproterozoic ductile shear zone fabrics (*c.* 1.75 Ga). Reactivation occurred at palaeodepths of 10–15 km, where frictional–viscous deformation synchronous with co-seismic frictional melting led to cycles of millimetre- to decimetre-scale cavity dilation and collapse. Although individual melt-generating slip surfaces may have become rapidly welded, faulting was able to repeatedly localize along adjacent pre-existing planar anisotropies favourably oriented for slip, leading to the creation of a mesh of foliation-parallel melt generation surfaces linked by foliation-perpendicular dilational voids. The latter features are filled by chaotic clast-supported wall rock collapse breccias, localized injected frictional melts and hydrothermal mineralization. The fills act as natural props, holding cavities open and preserving them as long-term, pipe-like fluid flow conduits. These exhumed features are likely to be typical of multi-rupture seismogenic fault systems formed by direct reactivation of pre-existing basement structures.

**Received** 11 March 2022; **revised** 6 October 2022; **accepted** 19 November 2022

A number of recent studies have emphasized the importance of near-surface dilatant fissure and void formation in areas where (mainly normal) faulting occurs in relatively strong, low-permeability rocks such as basalts, crystalline basement rocks and carbonates (e.g. Holland *et al.* 2006, 2011; van Gent *et al.* 2010; Walker *et al.* 2011; Weismüller *et al.* 2019; Hardman *et al.* 2020; Holdsworth *et al.* 2020*a*). Experimental testing and geomechanical modelling have shown that open voids can be stable to great depths, even in the absence of overpressure (e.g. Davis *et al.* 2017); for example, open cavities are known to exist below 8 km depth in several ultradeep hydrocarbon basins (e.g. Tarim Basin, China, Ukar *et al.* 2020). Such subterranean cavities have the potential to significantly influence the flow and storage of subsurface water, hydrothermal mineralizing fluids, magma and hydrocarbons. Therefore, research into fault-related void formation is of potential significance in the assessment of worldwide geological resources, geothermal reservoirs and geohazards.

Three related areas of current uncertainty are concerned with (1) how the development of these dilational phenomena may be related to seismogenic slip processes along brittle fault systems (e.g. Holdsworth *et al.* 2019), (2) understanding the depth range over which such dilational features may form along active crustal fault zones (e.g. Holland *et al.* 2011) and (3) understanding the preservation potential and mechanisms of deep void formation and filling. The well-exposed and accessible basement gneisses of the Neoarchean Lewisian Gneiss Complex in NW Scotland (Fig. 1) are an ideal location to explore some of these uncertainties. In these rocks, an array of geological processes can be examined that have occurred across a broad range of depths during a long history of deformation that spans close to three billion years. A series of distinct tectonic events are recognized, each associated with different *P*–*T* conditions broadly reflecting the apparent relative progressive exhumation of these rocks from the lower crust at *c.* 2.8 Ga to the surface by *c.* 1.2 Ga (Park 2005; Wheeler *et al.* 2010; MacDonald *et al.* 2015; Holdsworth *et al.* 2020*b*). The structures include very well-preserved examples of faults formed close to the frictional–viscous transition, which are widely associated with the development of pseudotachylytes (friction melts) (e.g. Sibson 1975; Beacom *et al.* 2001; Imber *et al.* 2001; Sibson and Toy 2006).

In this paper, we present field and microscopic observations, supported by stress inversion and fracture topology analyses from exceptionally well-exposed ancient seismogenic fault zones in Lewisian rocks from the Achmelvich area (Fig. 1). We show that these faults are particularly well developed in areas where pre-existing, steeply dipping to subvertical geological structures, such as foliations and dyke contacts, have been reactivated, and that in some cases large (up to decimetre-scale) dilational cavities were formed directly associated with ancient seismogenic faulting events. Although active cavity development may be transient at such great depths (*c.* 10–15 km), we show that geological processes can lead to natural (or self-) propping of partially open dilation sites (see Holdsworth *et al.* 2019; Cheng and Milsch 2021) that can then be preserved over long geological timescales. This has important potential implications for the fluid transport and storage properties, and the economic potential of crystalline basement terranes worldwide.

## Geological setting

The Precambrian rocks of the Lewisian Gneiss Complex, NW Scotland form a fragment of the continental basement of Laurentia that lies to the west of the Paleozoic Caledonian orogenic belt

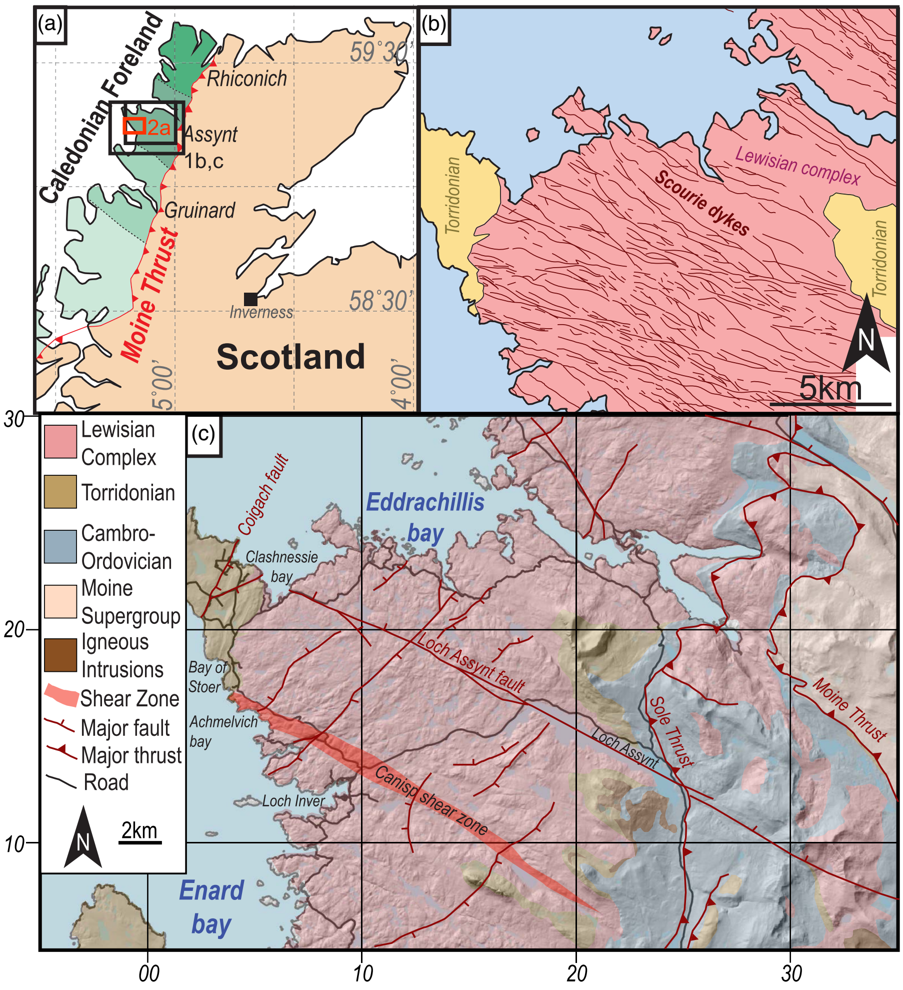

**Fig. 1.** (**a**) Simplified terrane map of the Lewisian complex west of the Moine Thrust. (**b**) Map showing local extent of the Scourie dyke swarm. (**c**) Geological map of the Assynt Terrane with hill shaded topography showing the Canisp shear zone and major faults. Source: Location maps, digital data provided with permission by EDINA Digimap (OS Terrain 5 (ASC & SHAPE geospatial data) scale 1:10 000, tiles NB92, NB91, NC01-03, NC11-13, NC21-23, NC31-33, updated April 2021, Ordnance Survey (GB), and DiGMapGB-50 (SHAPE geospatial data), scale 1:250 000, tiles NB92, NB91, NC01-03, NC11-13, NC21-23, NC31-33, updated April 2021, BGS, using EDINA Geology Digimap Service, https://digimap.edina.ac.uk); (b) adapted from Holdsworth *et al.* (2020*b*).

(Fig. 1). The rocks preserve evidence for a superimposed sequence of crustal-scale geological events that occurred from the Neoarchean to the present day (Sutton and Watson 1951; Park 1970; Park *et al.* 1994; Wheeler *et al.* 2010; McCaffrey *et al.* 2020).

The Assynt Terrane (Fig. 1a and b) forms the central part of the Lewisian Gneiss Complex in mainland NW Scotland. It is mostly composed of grey, banded, tonalite–trondhjemite–granodioritic (TTG) gneisses, which are locally highly heterogeneous in composition and include distinct mafic–ultramafic units (e.g. Sheraton *et al.* 1973; Guice *et al.* 2020). The TTG gneisses are thought to be derived from igneous plutons that were intruded into the crust at *c.* 2.85–3.03 Ga (high-precision U–Pb and Sm–Nd geochronology; Whitehouse 1989; Park 2005; Whitehouse and Kemp 2010; Whitehouse *et al.* 2022). These gneisses have subsequently undergone a series of Neoarchean to Mesopro terozoic deformation episodes prior to their final exhumation at the surface during the deposition of the overlying Stoer Group sediments in the Neoproterozoic (*c.* 1.2 Ga) (Beacom *et al.* 2001; Holdsworth *et al.* 2020*b*).

Following their initial emplacement as plutons, the basement rocks first experienced deformation and granulite-facies metamorphism (*c.* 1000°C, 11–15 kbar, *c.* 30 km depth) during the so-called Badcallian event(s), the timing of which is incompletely resolved (Wheeler *et al.* 2010; Whitehouse and Kemp 2010). Current age constraints suggest either a more widely favoured age of *c.* 2.76 Ga (e.g. Corfu *et al.* 1994; Zhu *et al.* 1997; MacDonald *et al.* 2015), and/or a younger age of *c.* 2.48–2.49 Ga (e.g. Friend and Kinny 1995; Kinny *et al.* 1999). In the central part of the Assynt Terrane, the generally flat-lying Badcallian structures are refolded and cross-cut by a steeply dipping, kilometre-scale NW–SE-trending zone of high-strain ductile deformation known as the Canisp Shear Zone (CSZ; Attfield 1987; Park and Tarney 1987; Fig. 1c). This dextral transpressional shear zone is thought to have developed initially during Inverian deformation and amphibolite-facies retrogression, which affected substantial parts of the Assynt Terrane (e.g. Evans and Lambert 1974; Attfield 1987). Mineral assemblages (Beach 1976) and deformation textures (Jensen 1984) suggest that significant exhumation had occurred since the Badcallian to depths in the range of 15–25 km (520–600°C). The absolute age of this event is also somewhat uncertain, but a majority of studies favour an age of *c.* 2.4 Ga (e.g. Corfu *et al.* 1994; Love *et al.* 2004; Goodenough *et al.* 2013).

The Badcallian and Inverian structures are cross-cut by a regionally extensive set of NW–SE-trending mafic and ultramafic intrusions known as the Scourie dyke suite (Fig. 1b). They are thought to have been emplaced under amphibolite-facies temperatures and pressures as a result of the autochthonous alteration of igneous pyroxenes to hornblende along the chilled margins of undeformed dykes (Tarney 1963; Scott 2018). Individual intrusions range in thickness from a few millimetres to several tens of metres and were intruded as two suites of differing age: a dominant *c.* 2.42–2.38 Ga set and a more minor group at *c.* 2.0 Ga (Rb–Sr whole-rock and U–Pb geochronology; Chapman 1979; Heaman and Tarney 1989; Davies and Heaman 2014).

The dykes and older structures in the host rock gneisses of the Assynt Terrane are cross-cut by a regional set of quartz–pyrite veins, the emplacement of which has been dated using Re–Os geochronology at *c.* 2.26 Ga (Vernon *et al.* 2014). These veins, and all older structures, are then heterogeneously overprinted by younger deformation with widespread retrogression of the TTG gneisses under lower amphibolite- to upper greenschist-facies metamorphic conditions (e.g. Sutton and Watson 1951; Attfield 1987; Beacom *et al.* 2001). This regionally recognized Laxfordian event begins with a series of magmatic and high-grade (upper amphibolite- to locally granulite-facies) events *c.* 1.9–1.87 Ga, followed by a protracted orogenic episode lasting from 1.79 to 1.66 Ga (see Park 2005; Goodenough *et al.* 2013). In the Assynt Terrane, the effects of Laxfordian reworking during dextral transpression are highly localized, being largely restricted to a 1 km wide zone at the centre of the CSZ and other, smaller local shear zones (e.g. Stoer shear zone), as well as along the margins of the Scourie dykes (Attfield 1987; Figs 1c and 2a). The phyllosilicate-rich mineralogy and deformation textures associated with dextral Laxfordian shear both in the central part of the CSZ and along dyke margins outside the CSZ are consistent with lowermost amphibolite- to greenschist-facies metamorphic conditions just below the frictional–viscous transition (*c.* 450–500°C, *c.* 15 km depth; Beach 1976; Jensen 1984; Attfield 1987; Chattopadhyay *et al.* 2010; Wilson *et al.* 2011; MacDonald *et al.* 2017).

In both the Assynt Terrane and the Gruinard Terrane to the SW (Fig. 1a), a younger set of strike-slip brittle–ductile shear zones, brittle faults and localized folds is recognized developed subparallel (NW–SE) to the pre-existing high-strain Laxfordian and Inverian fabrics, and the margins of many Scourie dykes (Shihe and Park 1993; Beacom *et al.* 2001; Holdsworth *et al.* 2020*b*) These structures are widely associated with the development of pseudotachylytes formed owing to rapid frictional melting during earthquake slip events along local fault zones. Rhenium–osmium geochronology of localized syntectonic copper–iron hydrothermal mineralization near Loch Assynt (Fig. 1c; Holdsworth *et al.* 2020*b*) yielded an age of *c.* 1.55 Ga for this faulting episode. Related epidote–quartz–chlorite mineralization is ubiquitous and, together with the typical depth range of most pseudotachylytes worldwide (Sibson and Toy 2006; Fagereng and Toy 2011), suggests that these faults probably formed under lower greenschist-facies conditions (*c.* 300–450°C) at depths of 10–15 km, close to the frictional–viscous transition assuming a standard continental geothermal gradient of 30°C $\text{km}^{-1}$. The associated NW–SE sinistral faults are kinematically distinct from the regional dextral displacements associated with significantly older Laxfordian deformation. Therefore Holdsworth *et al.* (2020*b*) have proposed that these *c.* 1.55 Ga structures are termed ‘Assyntian’ rather than the previously used term ‘Late Laxfordian’.

The Assyntian structures are post-dated by deposition of the unmetamorphosed and little-deformed *c.* 1.2 Ga Stoer Group sedimentary sequence (Holdsworth *et al.* 2020*b*; Killingback *et al.* 2020). This demonstrates that the currently exposed parts of the Lewisian Complex within the Assynt Terrane had been exhumed to the surface by that time. Regionally, both the Stoer Group and the wider Lewisian Complex are in turn unconformably overlain by younger Torridonian sequences thought to have been deposited no earlier than 1.04 Ga (Park *et al.* 1994).

The present study focuses on exceptionally well-exposed Assyntian fault zones found near the present-day coastline in the northern parts of Enard Bay in the Achmelvich–Stoer region (Figs 1c and 2a).

## Field and laboratory methods

### *Fieldwork, sampling and petrography*

Deformation structures affecting Lewisian gneisses and Scourie dykes were studied in the field using selected coastal outcrops from Lochinver to Clachtoll, and inland close to the north shore of Loch Assynt (Fig. 1c). The relative ages of country rock fabrics, igneous intrusions, mineral veins and fault rocks were ascertained from observed cross-cutting relationships. Structural geometries and kinematic relationships were recorded through collection of orientation and displacement vector data. Structural data were primarily collected in-field using compass–clinometers supplemented with orientation data derived from interpreted lineaments from orthorectified (planimetrically correct) virtual outcrop models and aerial imagery. Shear zone and later faulting kinematics were determined using ductile (asymmetric shear zone fabrics, porphyroclasts and S–C–C’ fabrics; e.g. Passchier and Trouw 2005) and brittle (offsets of piercing points, en echelon veins and slickenline steps; e.g. Petit 1987) shear sense criteria. A representative sample set of oriented hand specimens were collected for thin sectioning, and transmitted light microscopy was used to study petrography, microstructures and overprinting relationships.

### *Quantitative analysis of brittle structures*

Palaeostress inversions are a series of numerical and stereographic projection techniques that allow an approximation of the stress conditions that existed for a given set of coeval faults and fractures at the time of their formation using recorded fault vector data (i.e. slickenlines) (Angelier 1991). These techniques broadly assume that the slip vector data recorded in the field lie parallel to the shear component of the resolved stress tensor (Wallace 1951; Bott 1959). This assumption is reasonable if fault displacements are limited (finite strains low, with little rotation of fault blocks), a condition met by the small-displacement structures considered here. An analysis was undertaken on high-confidence slickenline data measured from 50 fault planes assigned to the Assyntian reactivation event across multiple outcrops in the CSZ and adjacent areas. Data were included in the sample set only if there was a clear indication of shear sense and were first corrected for later exhumation-related regional tilting (24° clockwise, around an axis of 00–007, derived from palaeodips of overlying Stoer Group strata) prior to inversion. Owing to the subvertical nature of the fault planes, the lineation data were recorded in the field as pitches or rakes on the fault plane to improve accuracy of data collection. The Improved Right Dihedron method based on that of Angelier and Mechler (1977) was applied using WinTensor software (Delvaux and Sperner 2003).

A slip tendency analysis was also carried out for the Assyntian faults as they are almost exclusively reactivations of pre-existing ductile foliations and dyke margins (see Morris *et al.* 1996; Lisle and Srivastava 2004; Dempsey *et al.* 2014, for background and rationale). The normalized slip tendency analysis defines the propensity of a measured plane to slip under the resolved stress field with an imposed (i.e. assumed) frictional coefficient (Morris *et al.* 1996; Lisle and Srivastava 2004). This analysis is presented as a ratio, where critically stressed fault orientations have a value close to unity and non-stressed faults have a value close to zero.

Fracture topology is a network characterization technique that simplifies a 2D fault or fracture network into discrete branches and nodes (Sanderson and Nixon 2015). It is used to define both the geometrical features and relationships between elements of a network and is a particularly useful way to describe fracture interconnectivity and therefore potential fluid transport properties. The ratios between different types of nodes (I–T or T–X; Isolated, Terminating, Cross-cutting), and branches can be used to determine the relative connectivity and spatial characteristics of the studied fracture network. In particular, $N_B/N_L$ ratios, the ratio of the number of fractures branches (fault trace between two nodes) versus the number of fault lengths (total faults between two tips or sampling boundaries) is used as a proxy for connectivity for a given fault network (Sanderson and Nixon 2015). In this study, fracture topology was calculated by hand from 2D planar images taken from a variety of scales, using orthorectified, planimetrically correct

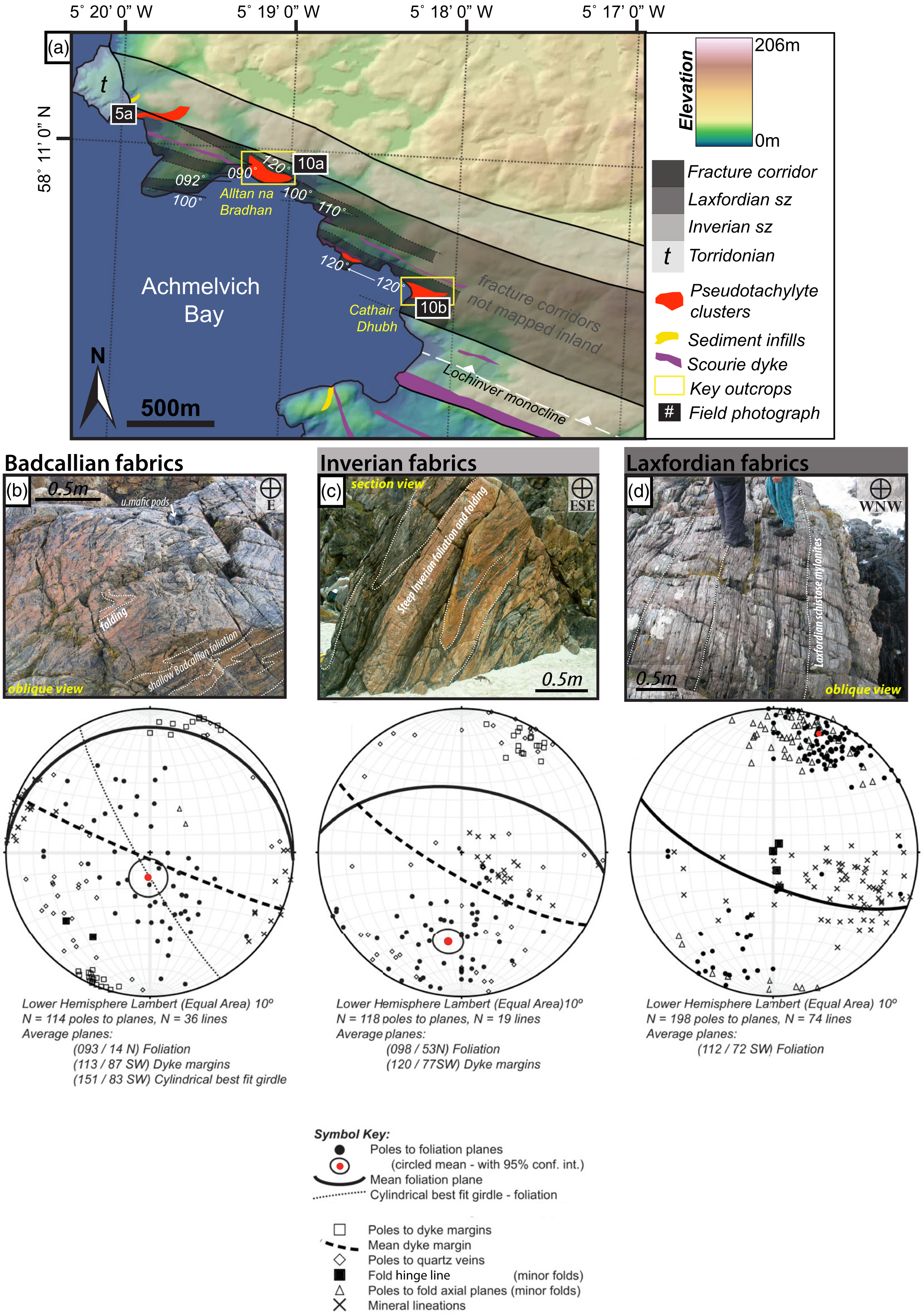

**Fig. 2.** Summary of pre-Assyntian ductile fabrics including representative field photographs, structural orientations and location map. (**a**) Location map showing the zonation of the Canisp Shear Zone at Achmelvich Bay and location of key Scourie dykes and structural data sources. sz, shear zone. (**b**) Above: field photograph of Badcallian foliation and schlieren textures around a mafic enclave (highlighted in white; [NC 0563 2500]). Below: lower hemisphere stereographic projection of Badcallian planar fabrics and lineation data, collected from outside the Canisp Shear Zone. (**c**) Above: field photograph of Inverian foliation and folding (highlighted in white; [NC 0575 2553]). Below: lower hemisphere stereographic projection of Inverian planar fabrics and lineation data, collected from the outer parts of the Canisp Shear Zone. (**d**) Above: field photograph of Laxfordian foliation (highlighted in white; [NC 0572 2554]). Below: lower hemisphere stereographic projection of Laxfordian planar fabrics and lineation data, collected from reactivated dyke contacts and central part of the Canisp Shear Zone.

fracture trace maps, generated from 3D virtual outcrop models of key localities (yellow boxes in Fig. 2a). The 3D models were built using structure-from-motion photogrammetry from photographs taken from a drone in Agisoft's Photoscan software, now called Metashape (e.g. Tavani *et al.* 2014). The generated models have sizes of 100 00$^2$ pixels with an effective viewing resolution of a few millimetres. Models were then interpreted manually using vector graphics software (Adobe Illustrator) at fixed zoom intervals using a single fixed resolution monitor to reduce bias and drift in interpretation density. This was necessary because of the exceptionally large number of fractures visible (>$10^5$ per model).

## Field and cross-cutting relationships

The earliest features preserved in the gneisses of the Achmelvich–Stoer region are best observed on the tidally exposed outcrops either side of Achmelvich Beach [NC 0549 2491 and NC 0568 2546] (Figs 1 and 2a, b). Shallowly NW- to north-dipping compositional layers (ranging from 1 mm to 100 cm thick) comprise alternating bands of mafic and leucocratic granodioritic to dioritic orthogneiss (Fig. 2b).

The amphibolite-facies Inverian event is represented within the study area by the steepening of the Badcallian foliation to form the Lochinver monocline (Evans and Lambert 1974) (Fig. 2a and c) and the development of the 1.5–2.5 km wide CSZ and its associated structures (Attfield 1987). This is a zone of intense NW–SE subvertical gneissic foliation (1–15 cm thick), tight minor folds and steeply obliquely plunging mineral lineations (Fig. 2c; Chattopadhyay *et al.* 2010).

The metadoleritic Scourie dykes cross-cut Badcallian and Inverian structures varying in width from centimetres to tens of metres and may extend laterally for many kilometres along-strike (Figs 1b, 2a and 3a). North of Achmelvich Beach [NC 0565 2507], a xenolith of foliated gneiss (40 × 170 cm) is encapsulated within an 30 m wide metadolerite dyke preserving the older Badcallian and Inverian fabrics within the gneiss (Fig. 3a and b). The original cross-cutting nature of the dykes is commonly partially to totally obscured by the development of later shear zones and faults that localize along and reactivate the dyke margins during Laxfordian and younger deformations (Wilson *et al.* 2011).

A central part of the CSZ *c.* 0.5 km wide is dominated by an overprinting Laxfordian ductile deformation (Fig. 2a), comprising subvertical high-intensity schistose fabrics (Fig. 2d). Scourie dykes here are transformed into amphibolites sheared into near concordance with the surrounding foliation in the gneisses (Figs 2d and 3c, d; e.g. [NC 0549 2491, NC 0568 2546]; Sheraton *et al.* 1973; Attfield 1987; Scott 2018). The subvertical NW–SE foliation is associated with shallowly plunging mineral lineations and widespread dextral shear criteria (Figs 2a, d and 3e) (Attfield 1987; Beacom *et al.* 2001; Wilson *et al.* 2011). The foliation locally anastomoses and coalesces around tight to isoclinal intrafolial (sheath) folds (Chattopadhyay *et al.* 2010), which act as local regions of lower strain where refolded Inverian or Badcallian folds and fabrics are locally preserved, together with cross-cutting amphibolites derived from otherwise transposed Scourie dykes (e.g. as seen on the coast at Port Alltan Na Bradhan; e.g. [NC 0479 2627]).

Dyke margins outside the CSZ also feature <20 cm wide developments of NW–SE schistose Laxfordian mylonites, in both the metadolerite and adjacent granitic gneiss (Fig. 3c and d; [NC 0549 2492, NC 0568 2546]). These schistose micaceous fabrics feature shallowly plunging mineral lineations, S–C fabrics (Fig. 3f) and asymmetric bending of foliations from regions of high strain to low strain that consistently demonstrate ductile dextral shear (Fig. 3d and e).

Steeply dipping to subvertical NW–SE brittle–ductile structures related to the Assyntian (previously ‘late-Laxfordian’) event localize along, and therefore reactivate, earlier ductile Laxfordian fabrics in the central part of the CSZ (Fig. 4a–c and along Scourie dyke margins (Figs 3c and 4d–f; Beacom *et al.* 2001; Holdsworth *et al.* 2020*b*). In the central CSZ, fault surfaces running parallel to or at low angles to the pre-existing schistose foliation preserve shallowly plunging slickenlines (Fig. 4g). Sinistral senses of shear are indicated by local offsets of markers, the development of shear band fabrics in phyllosilicate-rich horizons, the presence of dilational jogs, and by the development of millimetre- to

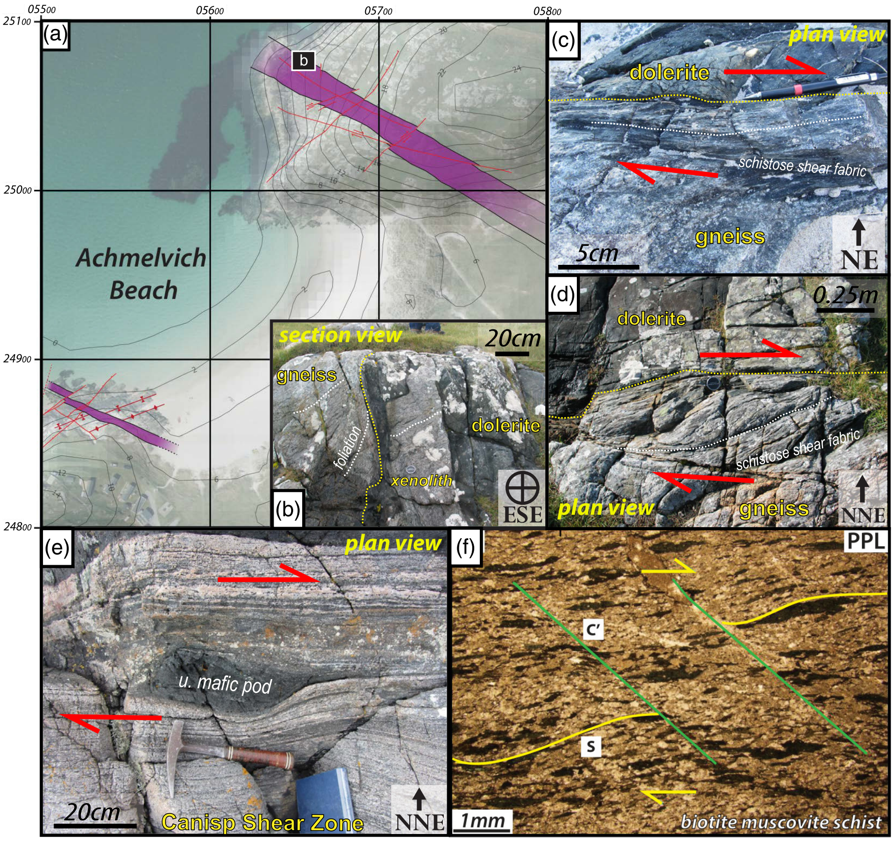

**Fig. 3.** Summary of dyke margin reactivation during the Laxfordian event. (**a**) Hill shaded topographic and satellite map of Achmelvich beach showing the present-day locations of two prominent Scourie dykes (purple) and surrounding structures. Data used with permission by EDINA Digimap (Aerial digimap, 25 cm resolution, 2018). Grid squares = 100 $m^2$. (**b**) Field photograph of gneiss xenolith within the northernmost dyke in (**a**). Gneissic foliation highlighted in white, and margins in yellow [NC 0565 2507]. (**c**) Field photograph of a ductile dextral sheared dyke margin from south side of Achmelvich beach, highlighting the development of centinetre-wide schistose shear fabrics (white dotted line) close to the pre-existing igneous contact (yellow dotted line; [NC 0546 2490]). (**d**) Field photograph of ductile dextrally sheared dyke margin, highlighting the development of asymmetrical schistose fabrics (white dotted line) on either side of the pre-existing igneous contact (yellow dotted line; [NC 0570 2512]). (**e**) Field photograph of asymmetric shear fabrics wrapping a pre-existing ultramafic pod [NC0473 2659]. (**f**) Thin section photomicrograph under plane-polarized light of dextral S–C’ (yellow and green) banding fabrics within the dyke-margin biotite muscovite schists.

centimetre-scale, steeply plunging, S-shaped folds (Fig. 4h). At the dyke margins, dextral ductile mylonites are overprinted by low-offset (<30 cm) brittle faults that host brecciated schistose material and low-angle slickenfibres that show sinistral offsets (Fig. 4d–f). These structures are widely associated with quartz–epidote–chlorite–hematite mineralization and local occurrences of ultra-mylonite and frictional melts (pseudotachylytes; e.g. Fig. 4f), all of which are consistent with their development under lower greenschist-facies metamorphic conditions close to, or just above the frictional–viscous transition (*c.* 300–450°C; 10–15 km depth).

The youngest features observed locally lie close (<5 m) to the basal breccia of the Clachtoll Formation, the oldest part of the unconformably overlying Stoer Group. At [NC 0416 2654], tensile fractures are filled with Stoer Group sediment and form a small network, with a subhorizontal <10 cm wide cavity, cutting two east–west-trending subvertical foliation-parallel fractures <6 cm wide (Fig. 5). The fracture cavities are evenly filled with three separate sedimentary packages subtly distinguished by differences in grain size and colour. These highly localized sediment-filled fractures are thought to have formed when clastic material was washed into local open fissures formed at the surface at *c.* 1.2 Ga (see also the features overlying the megaclast feature described at Clachtoll by Killingback *et al.* 2020).

## The geological characteristics of Assyntian reactivation

We focus first on the development of frictional–viscous Assyntian structures in the central part of the CSZ at Achmelvich as this represents the region where these structures are most intensely developed (e.g. Beacom *et al.* 2001; Wilson *et al.* 2011). We then briefly compare and contrast these features with equivalent-age structures that are locally developed along reactivated dyke margins outside the CSZ in the Achmelvich and Loch Assynt areas (Fig. 1c).

### *Central Canisp Shear Zone*

#### *Mesoscale features*

The Assyntian structures of the Canisp Shear Zone are dominated by two sets of mutually cross-cutting faults and fractures (Fig. 6a): a NW–SE-trending set of sinistral strike slip faults, formed sub-parallel to or at low angles to the pre-existing subvertical ductile foliation, and a dextral-extensional fault set trending NNE–SSW sub-perpendicular to the foliation (Figs 4b, c and 6a, b). Given their mutually cross-cutting behaviour, these faults are interpreted to be broadly coeval; they are, however, geologically distinct from one another. In all cases, however, the Lewisian host rocks adjacent to these fault sets (<2 cm from a fracture surface) are pervasively and distinctively stained dark red or brown owing to the percolation of iron-rich hematitic fluids throughout the fault network (e.g. Fig. 6b).

The sinistral NW–SE foliation-parallel faults are shear fractures with multi-metre displacements, as measured from offset markers where preserved. Hundreds, possibly thousands, of these faults are developed throughout the central part of the CSZ, with typical damage zones 2–6 cm wide (Beacom *et al.* 2001). Many, but not all, of these faults are locally associated with narrow continuous bands of pseudotachylyte (0.5–5 cm thick) developed along very long fault planes (ten to hundreds of metres), with the rare presence of small sinistrally verging folds (Figs 4b, h and 6c, d). Locally preserved slickenlines (Fig. 4g) are consistent with both sinistral and reverse slip offsets.

The NNE–SSW foliation-perpendicular faults rarely show shear offsets greater than a few centimetres. Where present, these demonstrate a minor dextral component to the slip (Fig. 6a). They are much wider in aperture than the foliation-parallel structures (up to tens of centimetres wide) with metre-wide damage zones defined by micro-fracture arrays and complex shapes (e.g. Fig. 6b, e and f). These foliation-perpendicular faults have much shorter lengths (typically 0.5–2 m) and are commonly bounded at their ends by foliation-parallel faults (Fig. 6f). A small number of foliation-perpendicular faults (e.g. at [NC 0486 2621]) have a longer trace length (e.g. up to 50 m) with greater shear offsets (up to a few metres) and appear to have formed from the linking together of several sets of foliation-perpendicular structures.

#### *Microscale features*

The foliation-parallel faults are associated with thin continuous veins of frictional melt: pseudotachylyte (Figs 4c and 7a). In thin section under high magnification, the pseudotachylytes show characteristic dendritic to spherulitic silica microcrystallites suspended in an amorphous dark matrix (Fig. 7b). This microstructure is consistent with a fast cooling rate (Kirkpatrick and Rowe 2013). Many melt-bearing, foliation-parallel shear fractures also display characteristic v-shaped injections or ‘wing-crack fills’ that are widely associated with pseudotachylyte developments globally (e.g. Fig. 7a, c and f; Di Toro *et al.* 2006; Rowe *et al.* 2018; Campbell *et al.* 2020). In some veins, clasts of older pseudotachylyte are preserved ‘floating’ in a matrix of younger frictional melt (Fig. 7g), and features interpreted to be injections are seen in outcrops locally cross-cutting one another, suggesting multiple phases of local seismicity and associated melting along discrete faults.

The foliation-parallel friction melts are locally exceptionally well exposed both in cross-section (Fig. 7c) and along-plane, and may display complex flow patterns (Fig. 7d). These flow striae are defined in outcrop by ridges and textures on the melt surface and by grain-size variation and clast frequency in thin section. The flow patterns show no clear orientation relationship to slickenlines, suggesting that they record the local migration of melt possibly driven by differences in pressure during seismogenic slip (Fig. 7d and e; Sibson 1975).

The foliation-perpendicular fractures show a highly diverse range of associated fills and are markedly dilational in character where bounded blocks are variably tilted and offset forming irregular ‘ladder fracture’ arrays (e.g. Fig. 6e and f). A range of heavily iron-stained breccias are developed with angular clasts of wall rock and variable volumes of finer grained matrix material (e.g. Figs 6e, f and 8a, b). Clast contents vary from 30 to 90% by volume, with the great majority being greater than 70%; thus, most are strongly clast supported. Following the terminology of Woodcock and Mort (2008), these fracture fills range from crackle breccias defined by approximately conjugate sets of shear fractures (Fig. 6b; the ‘ladder fractures’ of Beacom *et al.* 1999) to completely chaotic breccia made up of disaggregated collections of angular wall rock clasts bounded by relatively planar fractures on one or both sides (Figs 6e, f and 8a). The angular clasts range from 1 cm to tens of centimetres along their longest axis and show no sorting, preferred orientation or any uniform rotation direction. A variety of matrix fills are present (see below), but are commonly heavily iron-stained.

In a few localities, the foliation-perpendicular fractures also contain green epidote-cemented porous cataclasites and micro-breccias, particularly around Alltan Na Bradhan [NC 0486 2621] (Fig. 8b). These have lower clast contents (typically <30%) and appear to have formed where a greater degree of shear offset and attrition of clasts has occurred. Such less widespread, foliation-perpendicular faults have metre-scale dextral offsets and complex anastomosing and coalescing geometries with lengths of several tens to hundreds of metres.

Matrix fills comprise mineral cements and fine clasts of wall rock material. The mineralogy of the mineralization and fault rock cements is notably diverse (Fig. 8b–e). Limited cross-cutting relationships suggest that an earlier phase of cementation led to the

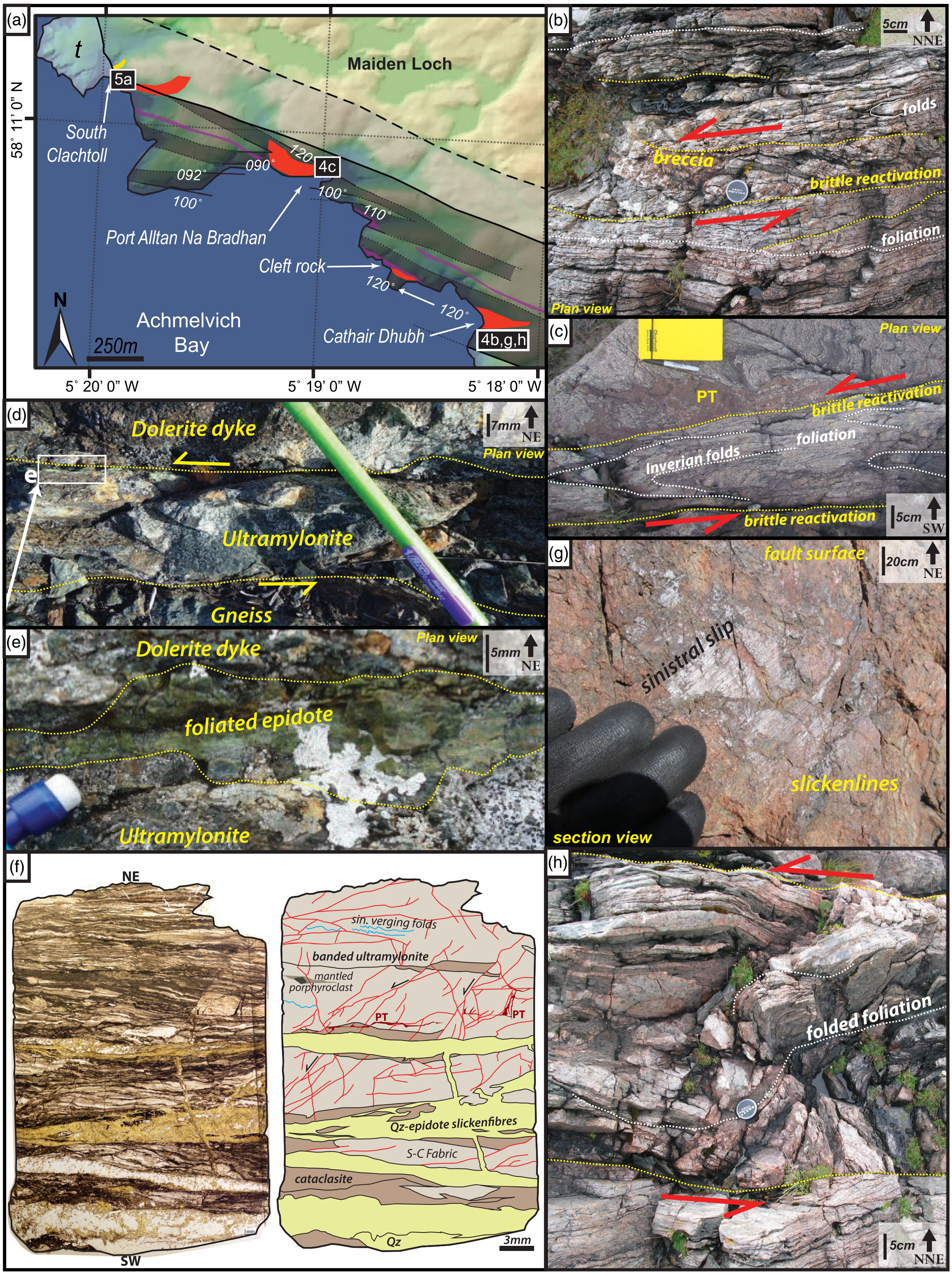

**Fig. 4.** Field photographs and maps summarizing the dyke margin and shear zone reactivation structures of the Assynt Terrane. (**a**) Location map showing the detailed zonation within the Canisp Shear Zone and locations of field photographs. (For key see Fig. 2a.) (**b**) Plan-view field photograph of foliation-parallel sinistral faults with breccia and hematite staining in schistose Laxfordian mylonites [NC 0572 2554]. (**c**) Field photograph of Inverian foliation and tight isoclinal folding (white) cut by foliation-parallel Assyntian faulting (yellow) associated with frictional melts, pseudotachylyte (PT; [NC 0416 2655]). (**d**) Field photograph of dyke margin Laxfordian ultramylonites in plan view overprinted by sinistral shear associated with epidote mineralization, Loch Assynt shore [NC 2104 2519]. (**e**) Field photograph from the same location as (**d**) showing detailed view of reactivated dyke margin contact highlighting sheared nature of epidote mineralization. (**f**) Thin section scan view and interpretation of dyke margin fabric taken at the Loch Assynt shoreline (after Holdsworth *et al.* 2020*b*). Section shows Assyntian ultramylonitic fabric with sinistral minor folds (blue), S–C fabrics and asymmetrically wrapped porphyroclasts, overprinted by sinistral cataclasites (brown), pseudotachylytes (PT), brittle faulting (red) and development of quartz–epidote mineralized slickenlines and attritional breccias (green). This tracks the development of dyke margin fabric across the frictional–viscous transition during the Assyntian. (**g**) Field photograph of slickenlines indicating sinistral shear sense on a NW–SE-trending foliation-parallel fault surface [NC 0575 2554]. (**h**) Plan-view field photograph of steeply plunging sinistral brittle–ductile folding associated with foliation-parallel detachments (yellow) with hematite staining in schistose Laxfordian mylonite. Trace of folded foliation shown in white [NC 0572 2554].

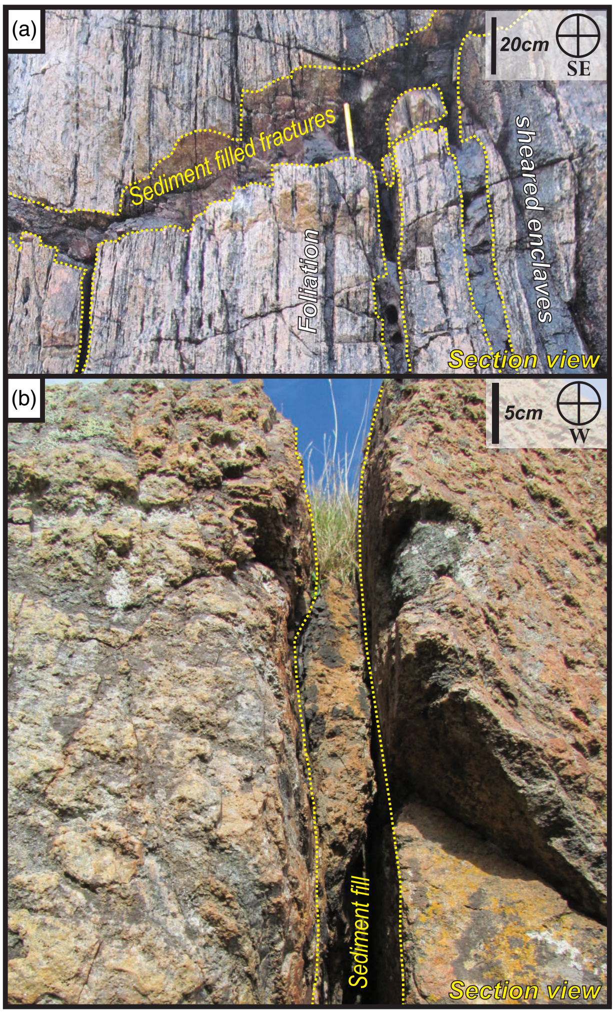

**Fig. 5.** Field photographs of sediment-filled faults and fractures. (**a**) Field photograph showing the sediment-filled fracture array highlighted in yellow [NC 0409 2659]. (**b**) Field photograph of sediment-filled fracture from the south side of Achmelvich Bay [NC 0534 2495].

development of hematite-cemented clasts of wall rock (Fig. 8d). A second phase of more complex epidote, pyrite, quartz, chalcedony, chlorite and prehnite mineralization is best seen in reactivated fault rocks, lining exposed fault walls (Fig. 8c and e–g). Regionally, epidote is always associated with Assyntian structures, and in the Loch Assynt locality Holdsworth *et al.* (2020*b*) have demonstrated that it is co-genetic with the sulfides that yielded the *c.* 1.55 Ga age using Re–Os geochronology. The youngest mineral fills are localized occurrences of calcite and zeolite veins. Despite the textural variation between the brecciated fault voids fills, they are all highly porous, and preserve significant vuggy cavities from a micro- to mesoscale (<1 mm up to 10 cm in diameter) (Fig. 8a and c).

A key feature seen in a number of foliation-parallel and foliation-perpendicular intersections is the presence of pseudotachylyte injections into abutting dilatant fractures and crackle breccias, akin to examples reported by Rowe *et al.* (2018). This shows that although the two sets of fractures are very different in their geological character, both are contemporaneous with, and therefore related to, the development of the same frictional melts during seismogenic slip. When viewed in thin section, the injected pseudotachylytes show vesicles, features that are seen only at these intersection points (Fig. 7h). These are thought to represent bubbles that formed from the near instantaneous depressurization of the melt following injection (e.g. Chernov *et al.* 2014).

### *Scourie dyke margins*

Many, but not all, exposed NW–SE-trending steeply dipping dyke margins show some evidence of reactivation during either Laxfordian and/or Assyntian deformation. Good examples of ductile dextral Laxfordian reactivation are preserved along the southern contact of the dyke exposed at [NC 0549 2491] and on the northern contact of the dyke at [NC 0568 2546] (Scott 2018), on the southern and northern sides of Achmelvich beach, respectively (Fig. 3a). Brittle fractures associated with both of these dykes (interpreted to be Assyntian) form two main sets: NW–SE-trending faults trending sub-parallel to dyke margins and a set of NE–SW-trending tensile fractures. These sets are mutually cross-cutting and abutting and are therefore interpreted to be coeval. The dyke margin-parallel shears host brecciated schistose material, and 1–5 cm thick bands of cataclasite associated with <2.5 cm thick pseudotachylytes, and a variety of different hydrothermal minerals (Fig. 4b–f). The cataclasites and breccia contain significant volumes of chlorite (15%), quartz (10%) and hornblende (15%) set in a quartzofeldspathic microcrystalline matrix (<10 µm grains). These brittle fabrics show offsets of gneissose banding, S–C fabrics, Riedel shears, kink-banding and shallowly plunging slickenlines, all of which indicate sinistral strike-slip (Fig. 4d–f). Adjacent to the dyke at [NC 0549 2491], tensile fractures within the gneiss trend NE–SW and are locally injected by <1 cm wide bands of frictional melt that originate from the prominent NW–SE fault that forms the northern margin of the dyke. Cross-cutting the pseudotachylytes and the dyke are pale-coloured zeolite veins trending ENE–WSW and in NE–SW-trending pull-apart features. The faulted dyke margin is prominently stained red–brown by hematite and this mineralization extends along fractures up to 3 m from the contact into the surrounding wall rock gneiss.

At Loch Assynt, 15 km east of Achmelvich, two subvertical dykes (40 and 10 m wide) sharply cross-cut the pre-existing gneissic foliation, and are in turn cut by a regional suite of (*c.* 2.26 Ga) quartz–pyrite veins (Vernon *et al.* 2014). Brittle reactivation of dyke margins by sinistral faults with associated Riedel shears is observed, marked locally by the development of 1–5 cm thick bands of dark foliated ultramylonites (Fig. 4f; [NC 2104 2519]; Holdsworth *et al.* 2020*b*). These ultra-fine-grained (0.1–0.5 mm) fault rocks feature S–C banding consistent with sinistral shear and are closely associated with narrow bands of frictional melt and quartz–epidote veining (*c.* 1 mm wide) (Fig. 4f). Millimetre-scale dilational jogs observed in the quartz–epidote veins both within the dyke and at the margins consistently indicate sinistral shear, and exposed vein margins exhibit sinistrally stepping quartz–epidote slickenfibres (Holdsworth *et al.* 2020*b*).

### *Palaeostress inversion analysis*

The principal stress axes derived from the stress inversion analysis indicate east–west compression and north–south extension. This is true for all data collected at Achmelvich (Fig. 9a) and also for a subset of those data from the exceptional set of exposures at Cathair Dhubh (Fig. 9b; location shown in Fig. 2a). The deduced stress axis orientations are consistent with strike-slip faulting and give almost identical results to the stress inversion analysis carried out on Assyntian structures at Loch Assynt (see Holdsworth *et al.* 2020*b*, fig. 9). The results of the slip tendency analysis show that steeply dipping, ESE-WNW planes oriented parallel to or at low angles to the foliation are most favourable for slip in the regionally determined stress field (Fig. 9c); this is consistent with the field observations and the development of the foliation-parallel shear fracture set. The Assyntian fractures seen within the collected kinematic data (see Figs 6a and 9a–c), including the foliation-perpendicular dextral faults and tensile sets, conform broadly to the

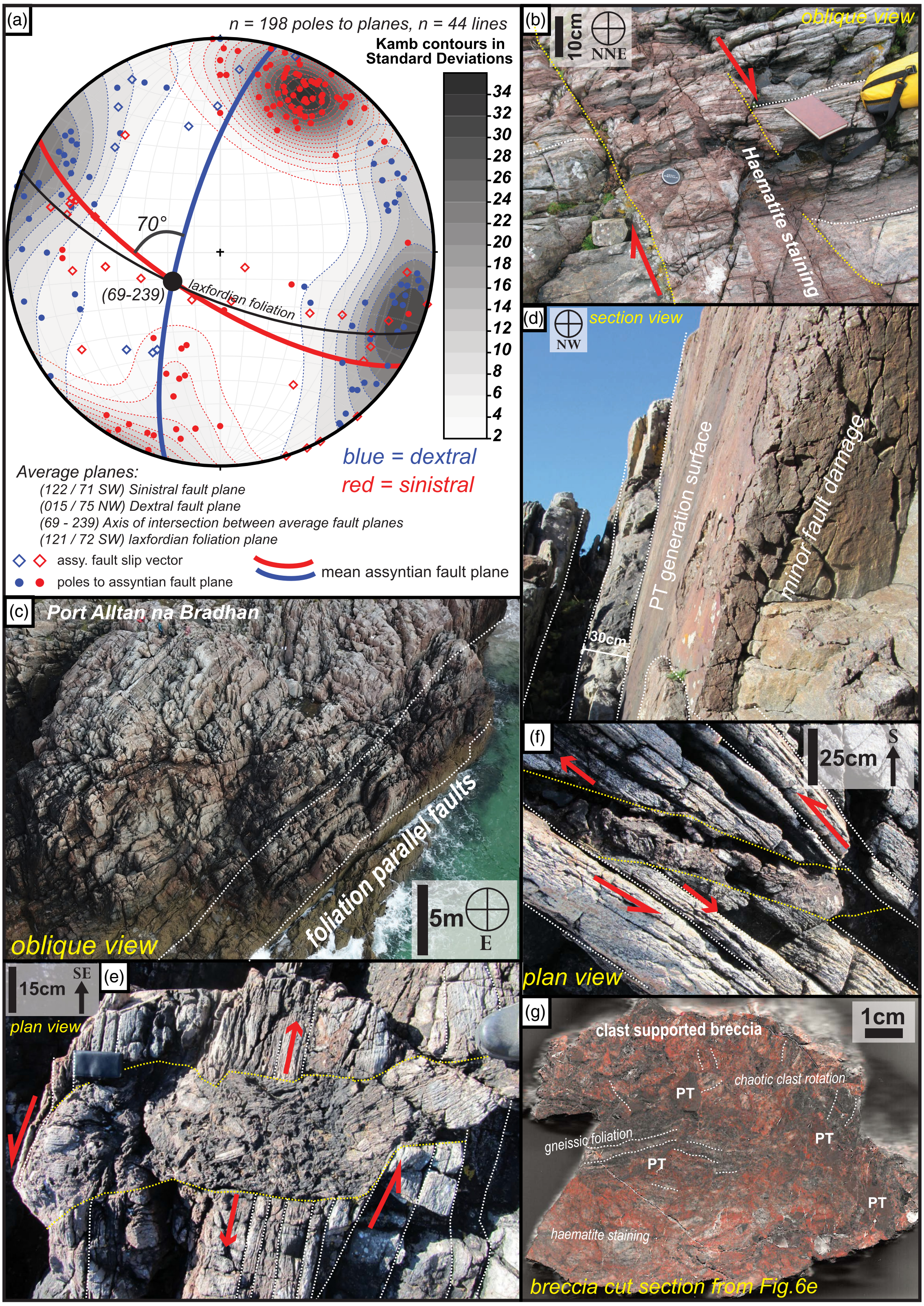

**Fig. 6.** Field photographs and orientation data from Alltan Na Bradhan and Cathair Dhubh outcrops, showing Assyntian fault architectures. Zones of foliation-perpendicular fractures are outlined in yellow; foliation planes and parallel shear faults are outlined in white. (**a**) Lower hemisphere stereographic projection of Assyntian fault planes. Data are divided into faults showing dextral (blue) and sinistral (red) offsets and are contoured independently and to the same scale. Poles to fault planes shown as circles with mean planes plotted and fault slip vectors as diamonds. Large black dot is the intersection lineation between sinistral and dextral mean fault planes. The mean Laxfordian foliation plane (from Fig. 2d) is also shown in black for reference. Kinematic data from these faults are shown in Figure 9. (**b**) Oblique field photograph of foliation-perpendicular 'ladder' fracture zone with pervasive hematite staining, multiple fractures and crackle breccias [NC 0483 2620]. (**c**) Oblique aerial image taken using a drone of the Port Alltan na Bradhan outcrop showing the large length, high intensity and minimal damage zone of the foliation-parallel Assyntian fractures [NC 0483 2620]. (**d**) Cross-section view in field photograph of foliation-parallel fault, featuring single discrete slip surface and minor damage zone on one fault wall [NC 0575 2553]. (**e**) Plan-view field photograph showing breccia-filled foliation-perpendicular fracture filled with chaotically rotated clasts and intra-clast void spaces [NC 0573 2554]. (**f**) Field photograph in plan view of dilatant breccia-filled fracture; the foliation-parallel opening vector orientation should be noted [NC 0573 2554]. (**g**) Cut sample showing chaotic, clast-supported nature of breccias, strong hematite staining and patches of injected pseudotachylyte.

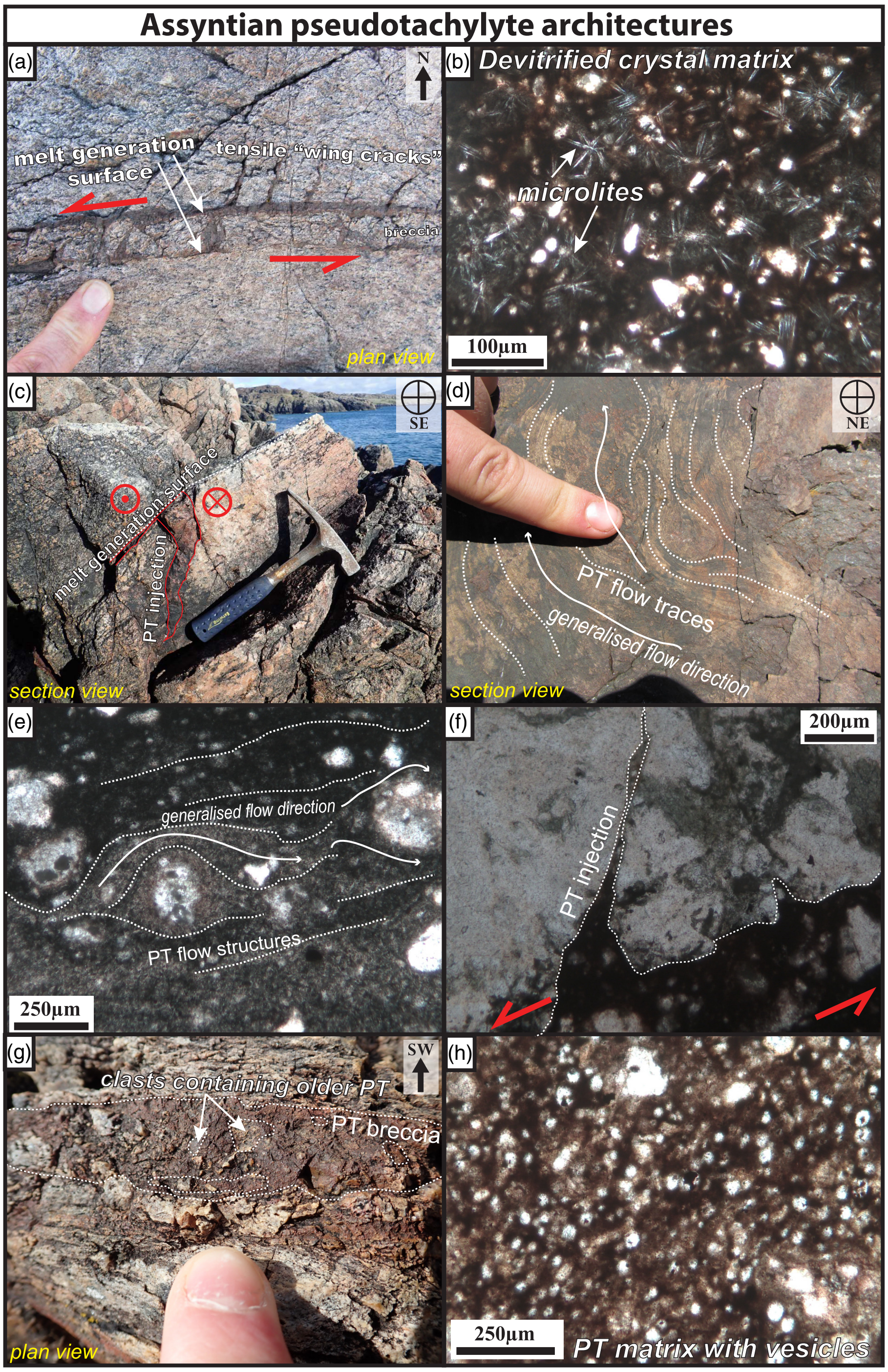

**Fig. 7.** Field photographs and photomicrographs of pseudotachylyte-bearing structures. (**a**) Plan view of composite pseudotachylyte injection vein and breccia showing numerous 'wing cracks' consistent with sinistral shear [NC 0415 2657]. (**b**) Thin section photomicrograph in plane-polarized light of devitrified pseudotachylyte showing dendritic–spherulitic silica microcrystallites set in an amorphous melt. (**c**) Cross-section view of large wing crack/injection vein of pseudotachylyte (outlined in red) emanating from a foliation-parallel fault (highlighted in white) [NC 0483 26200]. (**d**) Section view of pseudotachylyte in subvertical fault plane showing flow textures wrapping around fault plane asperities [NC 0575 2553]. (**e**) Thin section photomicrograph in plane-polarized light of flow structures within colour-banded composite pseudotachylyte. (**f**) Thin section photomicrograph in plane-polarized light of 'wing crack' injection into crystalline gneissic wall rock. (**g**) Close-up field photograph showing breccia with clasts of wall rock and early pseudotachylyte set in a matrix of younger pseudotachylyte melt [NC 0420 2657]. (**h**) Thin section photomicrograph in plane-polarized light of vesicles and amygdales in pseudotachylyte.

fracture criteria defined by Petit (1987). This suggests that the dextral foliation-perpendicular (R'), tensile (T) and more east–west-oriented sinistral faults (R) formed during sinistral shear along principal foliation-parallel faults (Y) (Fig. 9d and e).

### *Fracture topology*

To assess the fracture connectivity, fracture topology analyses were carried out using orthorectified fracture trace maps, generated from 3D virtual outcrop models of key well-exposed localities (Fig. 10). The results of these analyses showed that at all scales studied, the $N_B/N_L$ ratios were consistently >2.0, indicating a highly connected network. In addition, the results show a dominance of 'T' nodes over 'I' or 'X' and C–C type branches over I–C or I–I (Fig. 10, Table 1; for further details see Sanderson and Nixon 2015). This indicates that the fracture and fault systems here are very well connected at all scales. The high fracture intensity recorded within the Assyntian fault zones (locally up to 40 $m^{-1}$; see also Beacom *et al.* 2001), combined with the results of the topological analysis, show that the basement here is potentially exceptionally permeable to geological fluids, particularly in a subvertical direction parallel to the dominant fracture intersection orientation (Figs 6a and 9e).

## Discussion

### *Summary of field relationships*

The *c.* 1.55 Ga Assyntian deformation in the Achmelvich–Loch Assynt area is characterized by the sinistral reactivation of steeply dipping, pre-existing NW–SE-trending features including intrusive contacts of mafic dykes and Paleoproterozoic ductile shear zone fabrics. Reactivation occurred at palaeodepths interpreted to be in

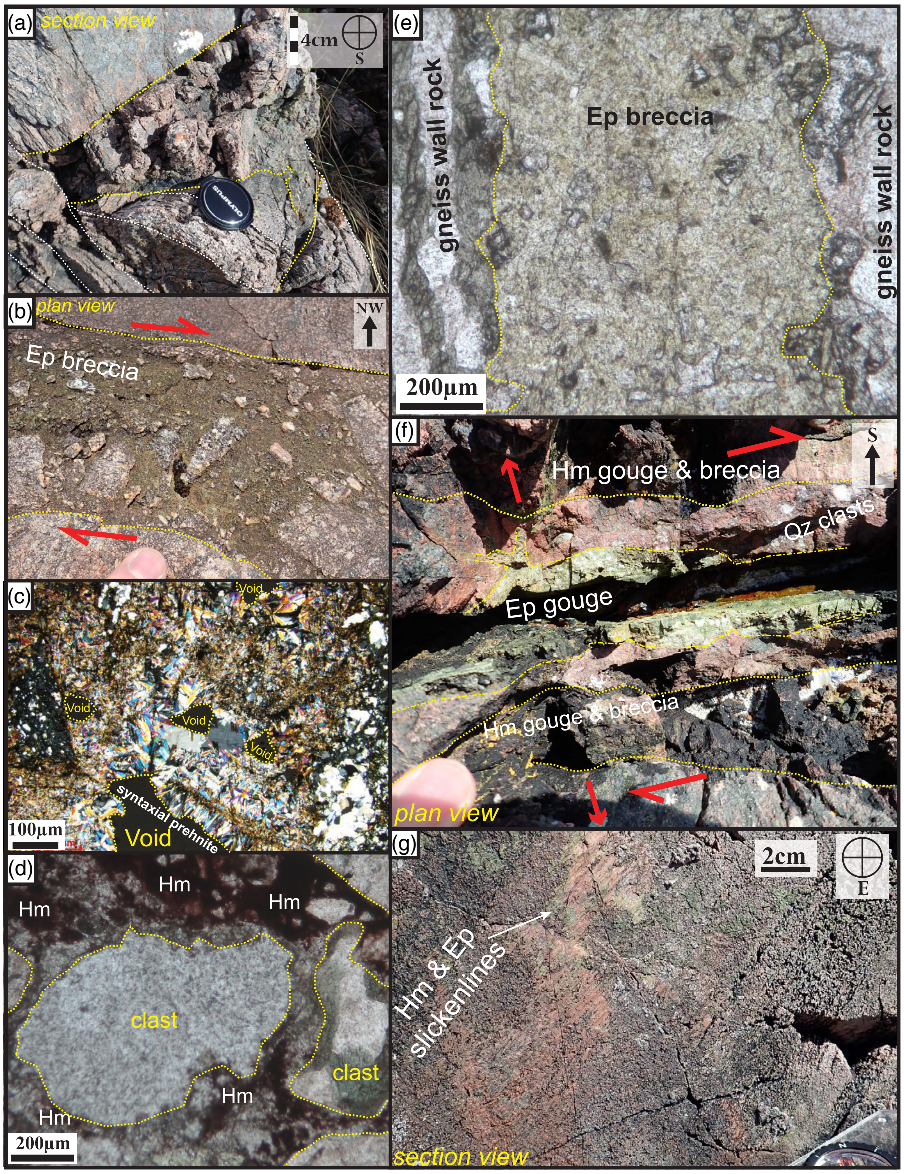

**Fig. 8.** Field photographs and thin sections of breccia fills. (**a**) Field photograph of breccia-filled foliation-perpendicular fracture (yellow) showing large cavities between clasts, abutting against foliation-parallel faults (white) [NC 0483 2620]. (**b**) Field photograph of foliation-perpendicular fault filled with angular clasts of wall rock set in an epidote-cemented matrix [NC 0482 2621]. (**c**) Thin section photomicrograph in crossed polars showing void spaces and syntaxial mineral growths of cementing prehnite. (**d**) Thin section photomicrograph in plane-polarized light of fault breccia showing hematite rims and cements around wall rock clasts. (**e**) Thin section photomicrograph in plane-polarized light of epidote-rich breccia–cataclasite between gneissic wall rock. (**f**) Field photograph of plan view of filled fault cavity showing multiple successive infills as distinguished by different clast types and mineral cements; earlier hematite cemented units are cut by later epidote cemented fault rocks [NC 0482 2621]. (**g**) Field photograph of foliation-parallel fault with preserved slickenlines showing epidote and hematite mineralized surfaces [NC 0482 2621].

the range 10–15 km based on palaeotemperature estimates. Faulting localizes along pre-existing planar anisotropies favourably oriented for left-lateral slip leading to the development of multiple foliation-parallel melt generation surfaces. In the phyllosilicate-rich CSZ, hundreds of these sub-parallel slip surfaces are linked by foliation-perpendicular (NE–SW) dilational voids and extensional or transtensional fractures (Fig. 11a). The latter features are filled by chaotic, clast-supported wall rock collapse breccias, localized injected frictional melts and a range of hydrothermal mineral fills.

### *The relative ages of the foliation-parallel and -perpendicular fracture sets*

The outcrops at Achmelvich–Clachtoll have previously been described by Beacom *et al.* (1999, 2001), who attributed the sinistral foliation- and dyke-parallel faulting to Assyntian (formerly ‘Late-Laxfordian’) deformation. However, those researchers suggested that the breccia-filled, foliation-perpendicular ‘ladder fractures’ within the CSZ were formed in the near-surface during transtensional faulting synchronous with deposition of the overlying Stoer Group. We disagree with this interpretation for three reasons.

(1) Foliation-perpendicular fractures are observed to be both cross-cut by and to cross-cut the foliation-parallel faults. This relationship was noted by Beacom *et al.* (1999), who suggested that some foliation-parallel faults were reactivated as transfer faults during Stoer Group-age rifting. Careful re-examination of all the outcrops suggests, however, that the mutual cross-cutting relationships are too ubiquitous to be interpreted in this way and that they can form only through episodic and contemporaneous deformation within a regionally consistent tectonic stress field, which the palaeostress analysis suggests is plausible.

(2) Frictional melts and veins that originate within the foliation-parallel faults are seen at several localities to be injected into dilatant foliation-perpendicular fractures (e.g. at [NC 0535 2576], [NC 0576 2554], [NC 0419 2659]). This can occur only if the latter are present and open(ing) during melt-generating slip events along the foliation-parallel faults. This observation was not made by Beacom *et al.* (1999), who correlated the foliation-perpendicular fractures with sediment-filled fractures seen close to the base of the Stoer Group at Clachtoll. We have been unable to find any sedimentary material in regions located more than a few metres from the Stoer Group, with the exception of a single breccia fill near an exposed hilltop at [NC 0534 2495]. Here a small 3–4 cm wide dilatant fracture is filled with a pale

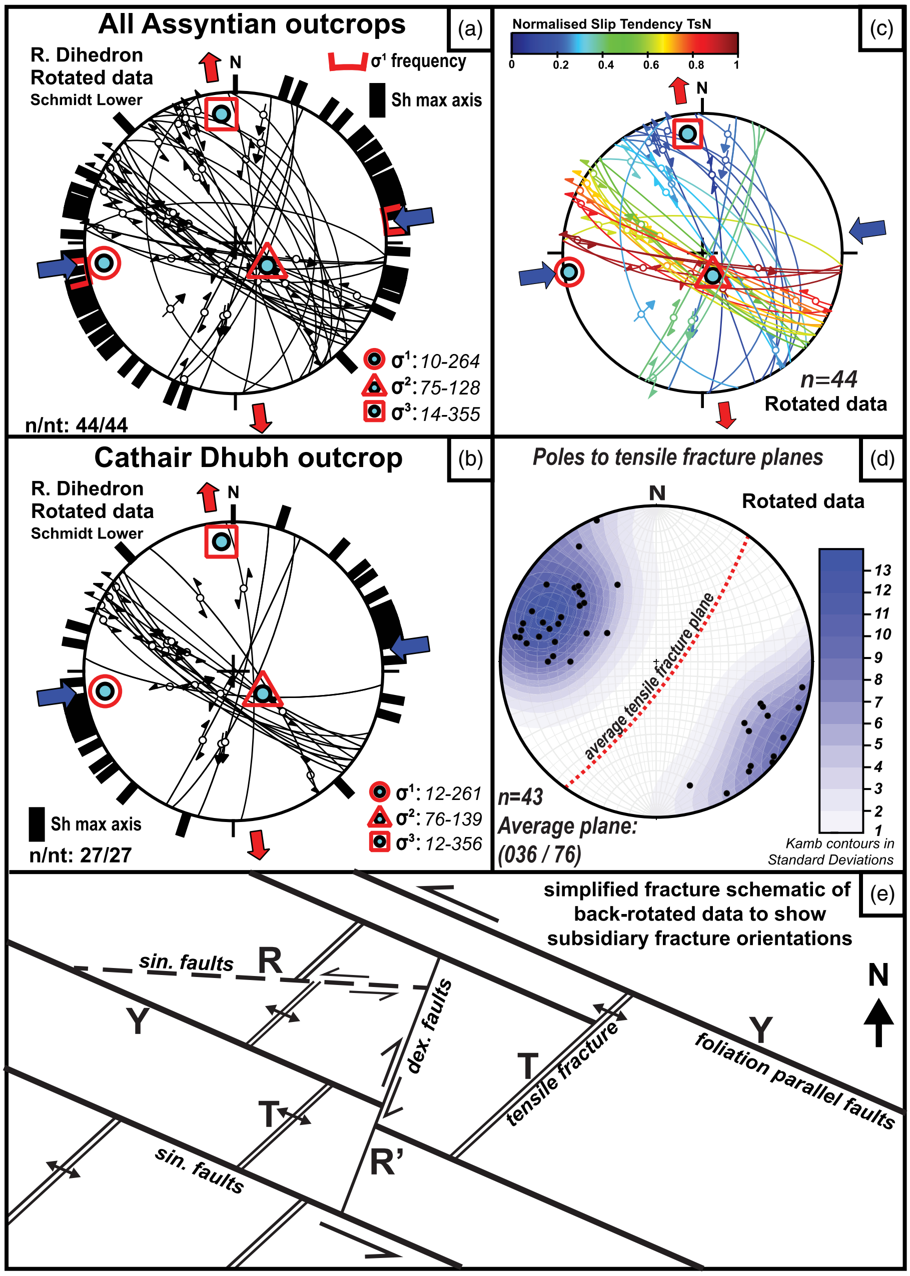

**Fig. 9.** Summary of inverted palaeostress axis orientations from slickenline data. In all cases, the data have been back-rotated to remove the regional tilt displayed by the immediately overlying Stoer Group (see Killingback *et al.* (2020)). It should be noted that the subvertical orientation of $\sigma_2$ is consistent with the proposed strike-slip regime. (**a**) Lower hemisphere stereographic projection of right dihedron palaeostress inversion results from all Assyntian outcrops. (**b**) Lower hemisphere stereographic projection showing the results of right dihedron palaeostress inversion from the Cathair Dhubh outcrop. (**c**) Stereographic projection showing results of normalized slip tendency analysis showing critically stressed east–west structures. (**d**) Lower hemisphere stereographic projection of contoured poles to observed tensile fault planes. (**e**) Schematic plan-view illustration showing the orientations of Assyntian faults and fractures in relation to Riedel secondary shear classifications: R, R', Y, T.

grey–tan sediment and breccia (Fig. 5b). This ESE–WNW fracture abuts a larger NNE–SSW-oriented fault, seen clearly in satellite imagery cutting the headland south of Achmelvich Bay. This sediment-filled fracture is interpreted to be a later exhumation-related feature associated with rifting and deposition of the Stoer Group in the near-surface. Notably, the sediment fill here lacks hematite staining and is oriented almost perpendicular to the Assyntian breccia-filled faults.

(3) The pervasive fracture- and microfracture-hosted iron-staining of the gneisses surrounding both the foliation-perpendicular and foliation-parallel faults suggests that the slip on both sets of faults was closely associated with the flux of iron-rich fluids, bearing in mind that this mineralization is texturally the earliest stage. This staining was also recognized by Beacom *et al.* (1999), but was attributed to the effects of younger near-surface fluid flow associated with rifting and deposition of the overlying Stoer Group sediments.

### *The importance of reactivation during seismogenic slip*

The Laxfordian and older structures of the Achmelvich–Clachtoll–Loch Assynt area show widespread evidence of reactivation during the *c.* 1.55 Ga Assyntian event, with brittle deformation and frictional melting related to seismogenic slip preferentially localized along prominent pre-existing mechanical anisotropies in the basement rocks. In the case of the CSZ, the Assyntian structures are strongly localized into the region of schistose mylonites related to ductile Laxfordian deformation (Fig. 11a). The rocks here are notably finer grained and are relatively enriched in well-aligned, relatively weak and anisotropic phyllosilicate minerals such as biotite, muscovite and chlorite. Given the findings of the slip tendency analysis, which shows that the steeply dipping, ESE–WNW-oriented foliation in the CSZ was favourably oriented for slip, it is probably not surprising that the Assyntian deformation preferentially localized in this region (see also the examples discussed by Peace *et al.* 2018).

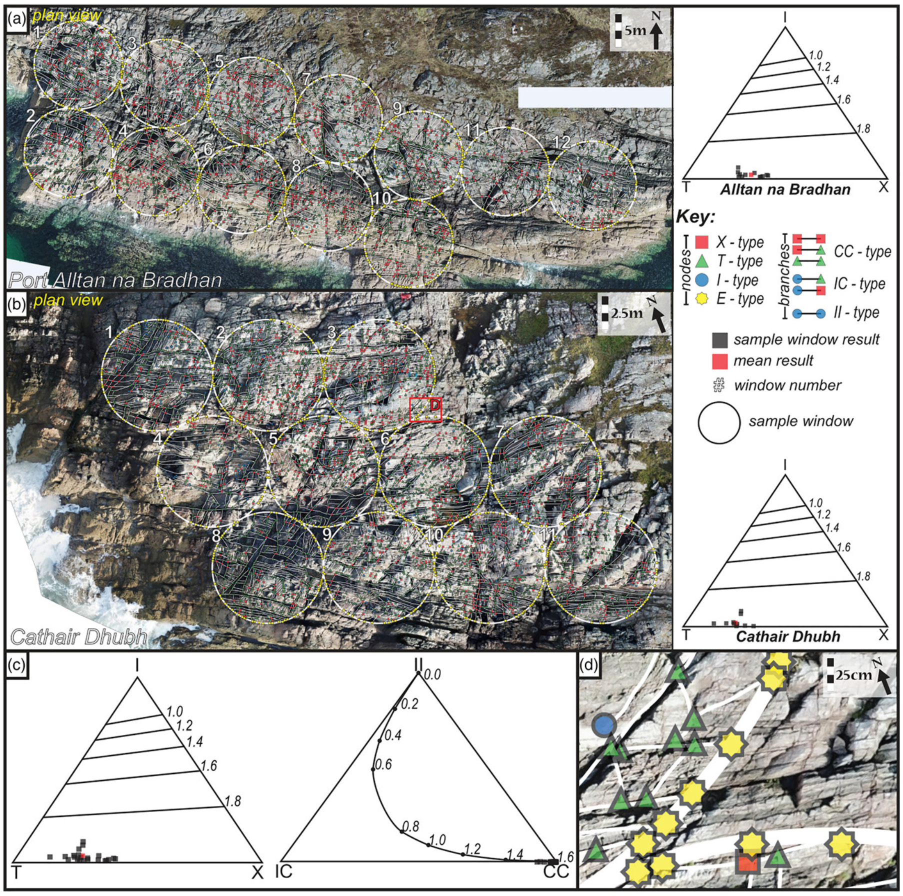

**Fig. 10.** Summary of fault topology from virtual outcrop models, after Sanderson and Nixon (2015). (**a**) Sample windows and topology superimposed onto a planimetrically correct orthorectified outcrop model of Alltan Na Bradhan. Right, topological results plotted onto a ternary diagram (Sanderson and Nixon 2015). (**b**) Sample windows and topology superimposed onto a planimetrically correct orthorectified outcrop model of Cathair Dhubh. (**c**) Summary of node and branch classifications from outcrops shown. (**d**) Maximum magnification of model in (**b**) showing the resolution of the model and extreme density of fractures present including uninterpreted fractures below viewing resolution during interpretation.

**Table 1.** *Table summarizing the results of topological analysis from the Cathair Dhubh (CD) and Alltan na Bradhan (AnB)*

| Sample | Cl | Cb | Node types (%) | | | Branch types (%) | | |
|---|---|---|---|---|---|---|---|---|
| | | | I | T | X | II | IC | CC |
| CD_1 | 4.000 | 1.941 | 9 | 67 | 24 | 0.2 | 5.9 | 94.0 |
| CD_2 | 4.448 | 1.984 | 3 | 74 | 24 | 0.0 | 1.6 | 98.4 |
| CD_3 | 4.778 | 1.994 | 1 | 65 | 34 | 0.0 | 0.6 | 99.4 |
| CD_4 | 3.551 | 1.929 | 11 | 66 | 23 | 0.0 | 7.1 | 92.9 |
| CD_5 | 4.457 | 1.994 | 1 | 73 | 26 | 0.0 | 0.6 | 99.4 |
| CD_6 | 4.225 | 1.979 | 3 | 74 | 23 | 0.0 | 2.1 | 97.9 |
| CD_7 | 4.587 | 1.992 | 1 | 69 | 30 | 0.0 | 0.8 | 99.2 |
| CD_8 | 3.764 | 1.983 | 3 | 84 | 14 | 0.0 | 1.7 | 98.3 |
| CD_9 | 3.950 | 1.982 | 3 | 77 | 20 | 0.0 | 1.8 | 98.2 |
| CD_10 | 4.365 | 1.986 | 2 | 72 | 25 | 0.0 | 1.4 | 98.6 |
| CD_11 | 4.282 | 1.993 | 1 | 77 | 22 | 0.0 | 0.7 | 99.3 |
| CD_Mean | 4.219 | 1.978 | 3 | 73 | 24 | 0.0 | 2.2 | 97.8 |
| AnB_1 | 4.521 | 1.980 | 3 | 64 | 33 | 0.0 | 2.0 | 98.0 |
| AnB_2 | 3.971 | 1.956 | 7 | 70 | 23 | 0.0 | 4.4 | 95.6 |
| AnB_3 | 4.811 | 1.993 | 1 | 61 | 38 | 0.0 | 0.7 | 99.3 |
| AnB_4 | 5.028 | 1.996 | 1 | 62 | 37 | 0.0 | 0.4 | 99.6 |
| AnB_5 | 5.145 | 1.991 | 2 | 58 | 41 | 0.0 | 0.9 | 99.1 |
| AnB_6 | 4.670 | 1.997 | 0 | 62 | 37 | 0.0 | 0.3 | 99.7 |
| AnB_7 | 4.364 | 1.996 | 1 | 73 | 27 | 0.0 | 0.4 | 99.6 |
| AnB_8 | 4.912 | 1.989 | 2 | 58 | 40 | 0.0 | 1.1 | 98.9 |
| AnB_9 | 4.294 | 1.985 | 2 | 71 | 26 | 0.0 | 1.5 | 98.5 |
| AnB_10 | 4.202 | 1.996 | 1 | 71 | 28 | 0.0 | 0.4 | 99.6 |
| AnB_11 | 4.174 | 1.987 | 2 | 69 | 29 | 0.0 | 1.3 | 98.7 |
| AnB_12 | 3.943 | 1.976 | 4 | 71 | 25 | 0.0 | 2.4 | 97.6 |
| AnB_Mean | 4.503 | 1.987 | 2 | 66 | 32 | 0.0 | 1.3 | 98.7 |
| Total mean | 4.367 | 1.983 | 3 | 69 | 28 | 0.0 | 1.7 | 98.3 |

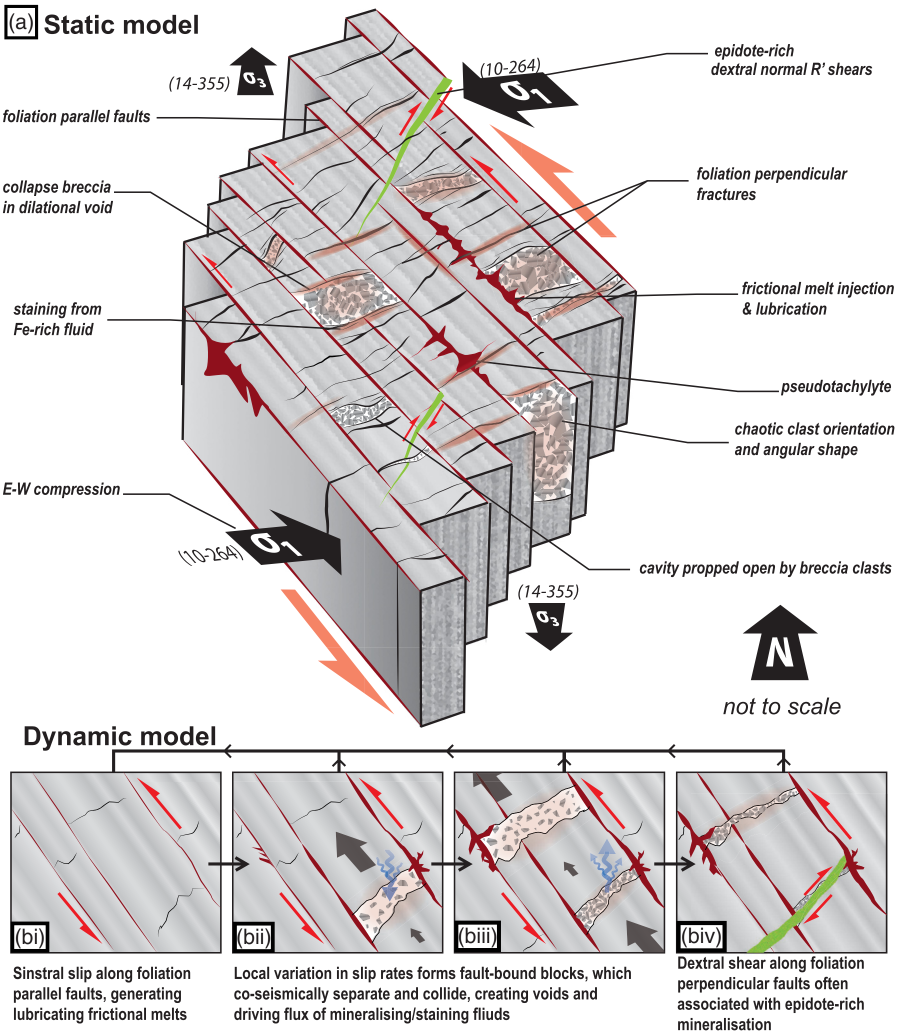

**Fig. 11.** (**a**) Summary 'static' 3D model of Assyntian reactivation structures (faults, fractures, fault rocks, mineralization) seen in the centre of the Canisp Shear Zone and the general relationship to sinistral shearing and the causative stresses (illustrated using $\sigma_1$ and $\sigma_3$ for reference). (**b**) (i–iv) Dynamic illustrative plan-view illustrations of sequential development and interactions of Assyntian structures showing the proposed block-shunting processes and relationships to frictional melting and fluid flow. It should be noted that the sequences may repeat and not always in the same order, as indicated by the black arrows connecting boxes.

Outside the CSZ, regionally developed features such as the Scourie dykes (Fig. 1c) are likely to represent an additional significant crustal-scale mechanical anisotropy. The observed localization of both Laxfordian and Assyntian deformation along many dyke margins, which are also in a favourable NW–SE orientation for slip, confirms that a crustal-scale anisotropy probably developed along intrusive contacts. Mantle-sourced regional dyke swarms are a common feature in basement terranes worldwide (e.g. Mackenzie dyke swarm, Canada; Hou *et al.* 2010). Given their origins as vertically oriented tensile fractures that cut much of the lithosphere, including the main load-bearing regions in the mid-crust, the localization of later regional deformation events along dyke margins is highly likely. Furthermore, many of the Scourie dyke margins were first deformed and retrogressed during Laxfordian ductile shearing, forming thin, dyke margin-parallel bands of schistose mylonite rich in weak, aligned phyllosilicates. This would probably make them even more prone to reactivation during later Assyntian strike-slip faulting.

The preferential reactivation of NW–SE dyke margins and ductile shear zone foliations is the result of strain partitioning and the development of a strong preferential alignment of slip generation surfaces and frictional melting (Fig. 11a). This highly organized configuration contrasts markedly with the patterns displayed by pseudotachylyte-bearing faults described from Lewisian rocks in the Outer Hebrides (Campbell *et al.* 2020). In the latter location, the faults show a diffuse distribution in terms of both location and orientation, a diverse range of orientations and a broad spectrum of senses of displacement including strike-slip, reverse and normal movements. This complexity may reflect a combination of superimposed deformation events over many tens of millions of years and/or may be due to the development of heterogeneous co-seismic stress field perturbations (Campbell *et al.* 2020). What is notable, however, is that widespread reactivation of pre-existing foliations by pseudotachylyte-bearing faults is not documented in the Outer Hebrides. The general absence of NW–SE steeply dipping dyke margins and shear zone fabrics in much of the Outer Hebrides may account for the lack of Assyntian-age reactivation structures and frictional melts in this region, highlighting the integral role of pre-existing basement foliation reactivation within the Assynt Terrane and similar settings globally (e.g. Di Toro and Pennacchioni 2005).

Field observations and rock deformation experiments (e.g. see Mitchell *et al.* 2016) have shown that solidified friction melts can weld seismic faults, making them stronger. This means that subsequent seismic ruptures may propagate along neighbouring pseudotachylyte-free slip surfaces, leading to long-term fault slip delocalization for successive ruptures. This suggestion is certainly consistent with the development of many hundreds of melt-generating slip surfaces all through the central part of the CSZ (Figs 2a and 11a) and other reactivated NW–SE shear zones in the Lewisian Gneiss Complex in mainland Scotland (e.g. see Beacom *et al.* 2001).

### *Void formation in the CSZ*

The close association between slip surfaces generating friction melts (the foliation-parallel faults) and coeval dilational foliation-perpendicular faults in the CSZ requires that their development is linked to seismogenic faulting processes at >10 km depth (Fig. 11a and b). We propose that shear failure was repeatedly localized along multiple foliation planes in the favourably oriented, highly anisotropic CSZ. It appears that simultaneous seismogenic slip and frictional melting occurred along adjacent foliation-parallel faults, allowing long, thin (1–20 cm thick; Beacom *et al.* 1999, 2001) slabs of host rock to have become transiently detached from one other. We propose that these melt-lubricated slabs were simultaneously pulled apart normal to the active slip surfaces generating the foliation-perpendicular fractures, leading to instantaneous implosion of the immediate wall rocks to form localized infills of crackle to chaotic collapse-breccia (e.g. Figs 6e, f and 11b (i, ii)). The chaotic arrangement of the breccia clasts in many examples implies that the initial dilational cavities must have been much larger to allow wall rock clasts to become so misoriented and disorganized. We therefore propose that subsequent co-seismic elastic rebound led to almost instantaneous partial closure of these fault-cavities. Importantly, however, the cavities were unable to close up completely as they were inevitably propped partially open by the infilling blocks of chaotically collapsed and misoriented wall rock (Fig. 11a and b).

Developing this concept further, we speculate that the melt-lubricated blocks may have moved co-seismically at variable relative velocities as slip was accommodated along different parts of the linked array of adjacent foliation-parallel faults. This could cause the detached blocks to move apart and collide relative to one another, rapidly opening and closing the foliation-normal fracture cavities, in some cases perhaps on multiple occasions (Fig. 11b(i–iv)). This is conceptually similar to shunting the carriages of a train, with each of the carriages represented by adjacent fault blocks, bound by the different types of fractures. Thus, if one block (carriage) was co-seismically shunted, it would move away from then adjacent block at its rear, and collide with the next adjacent block to the front, closing and opening the gaps between them (Fig. 11b(iii)). During opening, the cavity would be under a relative negative hydrostatic pressure and would draw in any available fluids, further fragments of wall rock or frictional melt. When a cavity collapsed, larger clasts would be held in place, propping open the cavity, and fluids or melt would be driven out, circulating fluid (and perhaps melt) throughout the adjacent fracture network (Fig. 11b(ii, iii)). It is significant that a greater proportion of frictional melt is observed along the foliation-parallel faults in regions where there are many associated tensile fractures, compared with those areas where foliation-normal fractures are sparse. One possible reason for this is that, during a seismic event, frictional melt was generated along the weak foliation-parallel faults, which lubricates multiple slip surfaces and facilitates the block dilation and shunting process.

## *Comparison with other examples of pseudotachylyte-bearing faults*

Pseudotachylyte occurs typically in associations of faults (or slip surfaces) and veins. The range in associations described by numerous researchers (e.g. Sibson 1975; Swanson 1989; Di Toro *et al.* 2006; Nielsen *et al.* 2008; Campbell *et al.* 2020) can be usefully compared with the ‘block-shunting’ model proposed here. The injection veins described by these researchers display a wide variety of shapes and architectures, including sigmoidal and curving lenses, blebs, ladders and networks; they are also associated with pseudotachylyte-filled breccias in seismically generated dilational jogs. These pull-apart features are in some respects similar to the foliation-normal fractures described in the present paper but exhibit two key differences. First, the dilation voids are commonly completely filled with friction melt. Second, the melt generation processes are not associated with hydrothermal mineralization, and there is no evidence for a long-lived cavity network, such as the preservation of open vugs as seen in the present examples.

Swanson (1989) described a process of ‘sidewall rip-out’ development, whereby localized transient variations in frictional resistance and therefore slipping velocity along a strike-slip fault trace causes the accumulation of stresses around ‘statically locked’ segments of a sliding fault, which if sufficient, can generate dilational tears (rip-outs) and secondary slip surfaces in the fault wall. In the examples described, the slipping surfaces generated frictional melts, which were then drawn into the rip-outs co-seismically under sub-lithostatic pressures. This has some similarity to the way in which frictional melt produced in the foliation-parallel faults at Achmelvich–Clachtoll–Loch Assynt is drawn into the abutting foliation-normal fractures as they open. Swanson (1989) further proposed that the generation of frictional melts facilitated the development of rip-outs as they lubricated the faults, allowing a rapid slip-rate; this too seems generally consistent with the co-seismic block-shunting behaviour observed in the examples described here. The outcrop pattern and mechanisms described necessitate multiple fault strands to be simultaneously ruptured, with fastest displacements being able to jump across from strand to strand.

## *Implications for the long-term preservation of deep void networks and fluid flow*

It is widely believed that substantially dilatant fracture cavities cannot exist below 1–2 km depth because of the inability of rocks to support the existence of open spaces at such high confining pressures. Our study demonstrates, however, that there is geological evidence to suggest that significant dilational cavities (centimetre scale) can form as co-seismic, transient features at depths >10–15 km. Furthermore, although they may collapse almost instantaneously, they can be preserved as partially open features owing to their being naturally propped open by chaotically entrained wall rock clasts. Although the causative faults may become inactive, these remaining voids within linked fault arrays can then provide pipe-like pathways for the migration of fluids, which probably explains their association in the Assynt Terrane with at least three phases of hydrothermal mineral fills: early ubiquitous hematite, followed by quartz–epidote–prehnite and lastly calcite and zeolite. Broadly speaking this mineralization sequence is consistent with a down-temperature history of fluid flow, but this remains to be tested more rigorously. It shoule be notedd that only limited amounts of fault reactivation are associated with the later calcite and zeolite mineralization, suggesting a predominantly passive filling related to younger regional faulting events. This lower temperature mineralization could be related to the final stages of Assyntian activity *c.* 1.5 Ga (Scott 2018) or could be associated with regional faulting as recently as the Mesozoic (e.g. McCaffrey *et al.* 2020). The fact that some may still preserve open vuggy cavities suggests that a proportion of the pore spaces created in the mid-crust were never fully occluded.

More tentatively, we suggest that the proposed kinematic model in Figure 11b presents a credible mechanism for the occurrence of a ‘seismogenic pumping’ process at significant depths. Although the boundary conditions here are quite specific, it is not unreasonable to suggest that other basement terranes that see seismogenic reactivation of highly anisotropic inherited fabrics might experience similar processes and may also see equivalent fluid or melt migration processes. For example, Holdsworth *et al.* (2019) have recently suggested that the migration of hydrothermal fluids and oil in the fractured basement reservoirs of the Rona Ridge west of Shetland was driven by a similar co-seismic pumping processes.

## Conclusions

The development of co-seismic, fault-hosted frictional melting and transient void formation is preserved in the basement rocks of the Lewisian Complex NW Scotland and formed during Mesoproterozoic (*c.* 1.55 Ga) strike-slip faulting. The deformation is characterized by sinistral reactivation of pre-existing NW–SE-trending Scourie dyke margins (*c.* 2.4 Ga) and ductile shear zone fabrics (Laxfordian, *c.* 1.75 Ga). In the CSZ, foliation-perpendicular, millimetre- to decimetre-scale cavities are commonly bounded by foliation-parallel, melt-coated slip surfaces. The cavities are occupied by chaotic wall rock collapse breccias, a locally diverse range of hydrothermal minerals, and less commonly by irregular patches of injected bubbly pseudotachylyte. The development of contemporaneous foliation-parallel and -perpendicular fracture meshes appears to reflect multiscale reactivation of the steeply dipping to subvertical pre-existing planar fabrics and dyke contacts during strike-slip movements. Whereas frictional melts rapidly cool and weld most of the foliation-parallel slip surfaces, the chaotic fills in the linking foliation-perpendicular voids act as natural (or self-) props holding cavities open. This preserves them as subvertical pipe-like fluid flow conduits over long geological time periods, as illustrated by the widespread development of broadly down-temperature hydrothermal mineralization in these brecciated cavities. The examples illustrate that mid-crustal void formation may initiate potentially very long-lived percolation pathways that are able to host later episodes of hydrothermal fluid flow and mineralization even if the hosting faults are not significantly reactivated.

**Acknowledgements** Thanks go to the Geological Society of London for its generous support of the research through the Annie Greenly Grant, and for publishing the field diary for this research in the *Geoscientist* magazine. We are grateful to the Tectonic Studies Group (TSG) for its travel bursary allowing the first author to present their work and gain valuable feedback from peers. The publishing of this work is funded by the Journal of the Geological Society ECR open-access prize. Thanks also go to all field assistants and helpers, and the authors' ever-patient partners.

**Author contributions** **KH**: data curation (lead), formal analysis (lead), investigation (lead), project administration (supporting), writing – original draft (lead), writing – review & editing (supporting); **REH**: conceptualization (lead), funding acquisition (lead), investigation (supporting), methodology (supporting), project administration (lead), resources (lead), supervision (lead), writing – original draft (supporting), writing – review & editing (lead); **LS**: data curation (supporting), investigation (supporting), writing – review & editing (supporting); **ED**: conceptualization (supporting), investigation (supporting), supervision (supporting), writing – review & editing (supporting); **KJWM**: conceptualization (supporting), investigation (supporting), supervision (supporting), writing – review & editing (supporting)

**Funding** This research was supported by the Annie Greenly Grant from the Geological Society of London. KH was self-funded.

**Competing interests** The authors declare that they have no known competing financial interests or personal relationships that could have appeared to influence the work reported in this paper.

**Data availability** All data generated or analysed during this study are included in this published article.

*Scientific editing by Martin Whitehouse*

## References

Angelier, J. 1991. Inversion directe et recherche 4-D: comparaison physique et mathematique de deux modes de determination des tenseurs des paleocontraintes en tectonique de failles. *Comptes Rendus - Academie des Sciences, Serie II*, **312**, 1213–1218.

Angelier, J.and Mechler, P. 1977. Sur une méthode graphique de recherche des contraintes principales également utilisables en tectonique et en séismologie: la méthode des dièdres droits. *Bulletin de la Société Géologique de France*, **S7-XIX**, 1309–1318, https://doi.org/10.2113/gssgfbull.S7-XIX.6.1309

Attfield, P. 1987. The structural history of the Canisp Shear Zone. *Geological Society, London, Special Publications*, **27**, 165–173, https://doi.org/10.1144/GSL.SP.1987.027.01.14

Beach, A. 1976. The interrelations of fluid transport, deformation, geochemistry and heat flow in early Proterozoic shear zones in the Lewisian Complex. *Philosophical Transactions of the Royal Society of London A*, **280**, 569–604, https://doi.org/10.1098/rsta.1976.0014

Beacom, L.E., Anderson, T.B.and Holdsworth, R.E. 1999. Using basement-hosted clastic dykes as syn-rifting palaeostress indicators: an example from the basal Stoer Group, northwest Scotland. *Geological Magazine*, **136**, 301–310, https://doi.org/10.1017/S0016756899002605

Beacom, L.E., Holdsworth, R.E., McCaffrey, K.J.W.and Anderson, T.B. 2001. A quantitative study of the influence of pre-existing compositional and fabric heterogeneities upon fracture-zone development during basement reactivation. *Geological Society, London, Special Publications*, **186**, 195–211, https://doi.org/10.1144/GSL.SP.2001.186.01.12

Bott, M.H.P. 1959. The mechanics of oblique slip faulting. *Geological Magazine*, **XCVI**, 109–117, https://doi.org/10.1017/S0016756800059987

Campbell, L.R., Lloyd, G.E., Phillips, R.J., Walcott, R.C.and Holdsworth, R.E. 2020. Stress fields of ancient seismicity recorded in the dynamic geometry of pseudotachylyte in the Outer Hebrides Fault Zone, UK. *Journal of the Geological Society, London*, **178**, jgs2020-101, https://doi.org/10.1144/jgs2020-101

Chapman, H.J. 1979. 2,390 Myr Rb–Sr whole-rock for the Scourie dykes of north-west Scotland. *Nature*, **277**, 642–643, https://doi.org/10.1038/277642a0

Chattopadhyay, A., Holdsworth, R.E., McCaffrey, K.J.W.and Wilson, R.W. 2010. Recording and analyzing geospatially accurate structural data through 'digital mapping' technique: a case study from the Canisp Shear Zone, NW Scotland. *Journal of the Geological Society of India*, **75**, 43–59, https://doi.org/10.1007/s12594-010-0023-y

Cheng, C.and Milsch, H. 2021. Hydromechanical investigations on the self-propping potential of fractures in tight sandstones. *Rock Mechanics and Rock Engineering*, **54**, 5407–5432, https://doi.org/10.1007/s00603-021-02500-4

Chernov, A.A., Kedrinsky, V.K.and Pil'nik, A.A. 2014. Kinetics of gas bubble nucleation and growth in magmatic melt at its rapid decompression. *Physics of Fluids*, **26**, 116602, https://doi.org/10.1063/1.4900846

Corfu, F., Heaman, L.M.and Rogers, G. 1994. Polymetamorphic evolution of the Lewisian complex, NW Scotland, as recorded by U–Pb isotopic compositions of zircon, titanite and rutile. *Contributions to Mineralogy and Petrology*, **117**, 215–228, https://doi.org/10.1007/BF00310864

Davies, J.H.F.L.and Heaman, L.M. 2014. New U–Pb baddeleyite and zircon ages for the Scourie dyke swarm: a long-lived large igneous province with implications for the Paleoproterozoic evolution of NW Scotland. *Precambrian Research*, **249**, 180–198, https://doi.org/10.1016/j.precamres.2014.05.007

Davis, T., Healy, D., Bubeck, A.and Walker, R. 2017. Stress concentrations around voids in three dimensions: the roots of failure. *Journal of Structural Geology*, **102**, 193–207, https://doi.org/10.1016/j.jsg.2017.07.013

Delvaux, D.and Sperner, B. 2003. New aspects of tectonic stress inversion with reference to the TENSOR program. *Geological Society, London, Special Publications*, **212**, 75–100, https://doi.org/10.1144/GSL.SP.2003.212.01.06

Dempsey, E.D., Holdsworth, R.E., Imber, J., Bistacchi, A.and Di Toro, G. 2014. A geological explanation for intraplate earthquake clustering complexity: the zeolite-bearing fault/fracture networks in the Adamello Massif (Southern Italian Alps). *Journal of Structural Geology*, **66**, 58–74, https://doi.org/10.1016/j.jsg.2014.04.009

Di Toro, G.and Pennacchioni, G. 2005. Fault plane processes and mesoscopic structure of a strong-type seismogenic fault in tonalites (Adamello batholith, Southern Alps). *Tectonophysics*, **402**, 55–80, https://doi.org/10.1016/j.tecto.2004.12.036

Di Toro, G., Hirose, T., Nielsen, S., Pennacchioni, G.and Shimamoto, T. 2006. Natural and experimental evidence of melt lubrication of faults during earthquakes. *Science*, **311**, 647–649, https://doi.org/10.1126/science.1121012

Evans, C.R.and Lambert, R.S.J. 1974. The Lewisian of Lochinver, Sutherland; the type area for the Inverian metamorphism. *Journal of the Geological Society, London*, **130**, 125–150, https://doi.org/10.1144/gsjgs.130.2.0125

Fagereng, Åand Toy, V.G. 2011. Geology of the earthquake source: an introduction. *Geological Society, London, Special Publications*, **359**, 1–16, https://doi.org/10.1144/SP359.1

Friend, C.R.L.and Kinny, P.D. 1995. New evidence for protolith ages of Lewisian granulites, northwest Scotland. *Geology*, **23**, 1027–1030, https://doi.org/10.1130/0091-7613(1995)023<1027:nefpao>2.3.co;2

Goodenough, K.M., Crowley, Q.G., Krabbendam, M.and Parry, S.F. 2013. New U–Pb age constraints for the Laxford Shear Zone, NW Scotland: evidence for tectono-magmatic processes associated with the formation of a Paleoproterozoic supercontinent. *Precambrian Research*, **233**, 1–19, https://doi.org/10.1016/j.precamres.2013.04.010

Guice, G.L., McDonald, I., Hughes, H.S.R., MacDonald, J.M.and Faithfull, J.W. 2020. Origin(s) and geodynamic significance of Archean ultramafic–mafic bodies in the mainland Lewisian Gneiss Complex, North Atlantic Craton. *Journal of the Geological Society, London*, **177**, 700–717, https://doi.org/10.1144/jgs2020-013

Hardman, K., Holdsworth, R.E., Dempsey, E.and McCaffrey, K. 2020. Nature and significance of rift-related, near-surface fissure-fill networks in fractured carbonates below regional unconformities. *Journal of the Geological Society, London*, **177**, 1168–1185, https://doi.org/10.6084/m9.figshare.c.5023103

Heaman, L.M.and Tarney, J. 1989. U-Pb baddeleyite ages for the Scourie dyke swarm, Scotland: evidence for two distinct intrusion events. *Nature*, **340**, 705–708, https://doi.org/10.1144/jgs2020-074

Holdsworth, R.E., McCaffrey, K.J.W. *et al.* 2019. Natural fracture propping and earthquake-induced oil migration in fractured basement reservoirs. *Geology*, **47**, 700–704, https://doi.org/10.1130/G46280.1

Holdsworth, R.E., Trice, R. *et al.* 2020*a*. The nature and age of basement host rocks and fissure fills in the Lancaster field fractured reservoir, West of Shetland. *Journal of the Geological Society, London*, **177**, 1057–1073, https://doi.org/10.1144/jgs2019-142

Holdsworth, R.E., Selby, D., Dempsey, E., Scott, L., Hardman, K., Fallick, A.E.and Bullock, R. 2020*b*. The nature and age of Mesoproterozoic strike-slip faulting base on Re–Os geochronology of syntectonic copper mineralisation, Assynt Terrane, NW Scotland. *Journal of the Geological Society, London*, **177**, 686–699, https://doi.org/10.1144/jgs2020-011

Holland, M., Urai, J.L.and Martel, S. 2006. The internal structure of fault zones in basaltic sequences. *Earth and Planetary Science Letters*, **248**, 286–300, https://doi.org/10.1016/j.epsl.2006.05.035

Holland, M., van Gent, H., Bazalgette, L., Yassir, N., Hoogerduijn Strating, E.H.and Urai, J.L. 2011. Evolution of dilatant fracture networks in a normal fault – evidence from 4D model experiments. *Earth and Planetary Science Letters*, **304**, 399–406, https://doi.org/10.1016/j.epsl.2011.02.017

Hou, G., Kusky, T.M., Wang, C.and Wang, Y. 2010. Mechanics of the giant radiating Mackenzie dyke swarm: a paleostress field modeling. *Journal of Geophysical Research*, **115**, B02402, https://doi.org/10.1029/2007JB005475

Imber, J., Holdsworth, R.E., Butler, C.A. and Strachan, R.A. 2001. A reappraisal of the Sibson-Scholz fault zone model: The nature of the frictional to viscous ('brittle-ductile') transition along a long-lived crustal-scale fault, Outer Hebrides, Scotland. *Tectonics*, **20**, 601–624, https://doi.org/10.1029/2000TC001250

Jensen, L.N. 1984. Quartz microfabric of the Laxfordian Canisp Shear Zone, NW Scotland. *Journal of Structural Geology*, **6**, 293–302, https://doi.org/10.1016/0191-8141(84)90053-1

Killingback, Z., Holdsworth, R.E., Walker, R.J., Nielsen, S., Dempsey, E. and Hardman, K. 2020. A bigger splat: The catastrophic geology of a 1.2 billion year old terrestrial megaclast, NW Scotland. *Geology*, **49**, 180–184, https://doi.org/10.1130/G48079.1

Kinny, P.D., Friend, C.R.L., Strachan, R.A., Watt, G.R.and Burns, I.M. 1999. U–Pb geochronology of regional migmatites in East Sutherland, Scotland: evidence for crustal melting during the Caledonian orogeny. *Journal of the Geological Society, London*, **156**, 1143–1152, https://doi.org/10.1144/gsjgs.156.6.1143

Kirkpatrick, J.D.and Rowe, C.D. 2013. Disappearing ink: how pseudotachylytes are lost from the rock record. *Journal of Structural Geology*, **52**, 183–198, https://doi.org/10.1016/j.jsg.2013.03.003

Lisle, R.J.and Srivastava, D.C. 2004. Test of the frictional reactivation theory for faults and validity of fault-slip analysis. *Geology*, **32**, 569–572, https://doi.org/10.1130/G20408.1

Love, G.J., Kinny, P.D.and Friend, C.R.L. 2004. Timing of magmatism and metamorphism in the Gruinard Bay area of the Lewisian Gneiss Complex: comparisons with the Assynt Terrane and implications for terrane accretion. *Contributions to Mineralogy and Petrology*, **146**, 620–636, https://doi.org/10.1007/s00410-003-0519-1

MacDonald, J.M., Goodenough, K.M., Wheeler, J., Crowley, Q., Harley, S.L., Mariani, E.and Tatham, D. 2015. Temperature–time evolution of the Assynt Terrane of the Lewisian Gneiss Complex of Northwest Scotland from zircon U–Pb dating and Ti thermometry. *Precambrian Research*, **260**, 55–75, https://doi.org/10.1016/j.precamres.2015.01.009

MacDonald, J.M., Magee, C. and Goodenough, K.M. 2017. Dykes as physical buffers to metamorphic overprinting: an example from the Archaean–Palaeoproterozoic Lewisian Gneiss Complex of NW Scotland. *Scottish Journal of Geology*, **53**, 41–52, https://doi.org/10.1144/sjg2017-004

McCaffrey, K.J.W., Holdsworth, R.E., Pless, J., Franklin, B.S.G. and Hardman, K. 2020. Basement reservoir plumbing: fracture aperture, length and topology analysis of the Lewisian Complex, NW Scotland. *Journal of the Geological Society, London*, **177**, 1281–1293, https://doi.org/10.1144/jgs2019-143

Mitchell, T.M., Toy, V., Di Toro, G., Renner, J. and Sibson, R.H. 2016. Fault welding by pseudotachylyte formation. *Geology*, **44**, 1059–1062, https://doi.org/10.1130/G38373.1

Morris, A., Ferrill, D.A. and Henderson, D.B. 1996. Slip-tendency analysis and fault reactivation. *Geology*, **24**, 275–278, https://doi.org/10.1130/0091-7613(1996)024<0275:STAAFR>2.3.CO;2

Nielsen, S., Di Toro, G., Hirose, T. and Shimamoto, T. 2008. Frictional melt and seismic slip. *Journal of Geophysical Research*, **113**, B01308, https://doi.org/10.1029/2007JB005122

Park, R.G. 1970. Observations on Lewisian Chronology. *Scottish Journal of Geology*, **6**, 379–399, https://doi.org/10.1144/sjg06040379

Park, R.G. 2005. The Lewisian terrane model: a review. *Scottish Journal of Geology*, **41**, 105–118, https://doi.org/10.1144/sjg41020105

Park, R.G. and Tarney, J. 1987. The Lewisian complex: a typical Precambrian high-grade terrain? *Geological Society, London, Special Publications*, **27**, 13–25, https://doi.org/10.1144/gsl.sp.1987.027.01.03

Park, R.G., Cliff, R.A., Fettes, D.J. and Stewart, A.D. 1994. Precambrian rocks in northwest Scotland west of the Moine Thrust. *In*: Gibbons, W. and Harris, A.L. (eds) *A Revised Correlation of Pre-Cambrian Rocks in the British Isles*. Geological Society, London, 6–22, https://doi.org/10.1144/sr22.2

Passchier, C.W. and Trouw, R.A.J. 2005. *Microtectonics*, 2nd edn. Springer, Berlin.

Peace, A., McCaffrey, K., Imber, J., van Hunen, J., Hobbs, R. and Wilson, R. 2018. The role of pre-existing structures during rifting, continental breakup and transform system development, offshore West Greenland. *Basin Research*, **30**, 373–394, https://doi.org/10.1111/bre.12257

Petit, J.P. 1987. Criteria for the sense of movement on fault surfaces in brittle rocks. *Journal of Structural Geology*, **9**, 597–608, https://doi.org/10.1016/0191-8141(87)90145-3

Rowe, C.D., Ross, C. *et al.* 2018. Geometric complexity of earthquake rupture surfaces preserved in pseudotachylyte networks. *Journal of Geophysical Research: Solid Earth*, **123**, 7998–8015, https://doi.org/10.1029/2018JB016192

Sanderson, D.J. and Nixon, C.W. 2015. The use of topology in fracture network characterization. *Journal of Structural Geology*, **72**, 55–66, https://doi.org/10.1016/j.jsg.2015.01.005

Scott, L.J. 2018. *Dyke reactivation across the frictional–viscous transition: Precambrian deformation of Scourie dyke margins in NW Scotland*. Masters thesis, Durham University.

Sheraton, J., Skinner, A. and Tarney, J. 1973. The Geochemistry of the Scourian gneisses of the Assynt district. *In*: Park, R. and Tarner, J. (eds) *The Early Precambrian of Scotland and Related Rocks of Greenland*. University of Keele, 13–30.

Shihe, L. and Park, R.G. 1993. Reversals of movement sense in Lewisian brittle–ductile shear zones at Gairloch, NW Scotland, in the context of Laxfordian kinematic history. *Scottish Journal of Geology*, **29**, 9–19, https://doi.org/10.1144/sjg29010009

Sibson, R.H. 1975. Generation of Pseudotachylyte by Ancient Seismic Faulting. *Geophysical Journal of the Royal Astronomical Society*, **43**, 775–794, https://doi.org/10.1111/j.1365-246X.1975.tb06195.x

Sibson, R.H. and Toy, V.G. 2006. The habitat of fault-generated pseudotachylyte: presence vs. absence of friction-melt. *Geophysical Monograph, American Geophysical Union*, **170**, 153–166, https://doi.org/10.1029/170GM16

Sutton, J. and Watson, J. 1951. The pre-Torridonian metamorphic history of the Loch Torridon and Scourie areas in the North-West Highlands, and its bearing on the chronological classification of the Lewisian. *Quarterly Journal of the Geological Society of London*, **106**, 241–307, https://doi.org/10.1144/GSL.JGS.1950.106.01-04.16

Swanson, M.T. 1989. Sidewall ripouts in strike-slip faults. *Journal of Structural Geology*, **11**, 933–948, https://doi.org/10.1016/0191-8141(89)90045-X

Tarney, J. 1963. Assynt dykes and their metamorphism. *Nature*, **199**, 672–674, https://doi.org/10.1038/199672a0

Tavani, S., Granado, P. *et al.* 2014. Building a virtual outcrop, extracting geological information from it, and sharing the results in Google Earth via OpenPlot and Photoscan: an example from the Khaviz Anticline (Iran). *Computers and Geosciences*, **63**, 44–53, https://doi.org/10.1016/j.cageo.2013.10.013

Ukar, E., Baqués, V., Laubach, S.E. and Marrett, R. 2020. The nature and origins of decameter-scale porosity in Ordovician carbonate rocks, Halahatang oilfield, Tarim Basin, China. *Journal of the Geological Society, London*, **177**, 1074–1091, https://doi.org/10.1144/jgs2019-156

van Gent, H.W., Holland, M., Urai, J.L. and Loosveld, R. 2010. Evolution of fault zones in carbonates with mechanical stratigraphy – insights from scale models using layered cohesive powder. *Journal of Structural Geology*, **32**, 1375–1391, https://doi.org/10.1016/j.jsg.2009.05.006

Vernon, R., Holdsworth, R.E., Selby, D., Dempsey, E., Finlay, E. and Fallick, A.J. 2014. Structural characteristics and Re–Os dating of quartz–pyrite veins in the Lewisian Gneiss Complex, NW Scotland: evidence of an Early Paleoproterozoic hydrothermal regime during terrane amalgamation. *Precambrian Research*, **246**, 256–267, https://doi.org/10.1016/j.precamres.2014.03.007

Walker, R.J., Holdsworth, R.E., Imber, J. and Ellis, D. 2011. The development of cavities and clastic infills along fault-related fractures in Tertiary basalts on the NE Atlantic margin. *Journal of Structural Geology*, **33**, 92–106, https://doi.org/10.1016/j.jsg.2010.12.001

Wallace, R.E. 1951. Geometry of shearing stress and relation to faulting. *Journal of Geology*, **59**, 118–130, https://doi.org/10.1086/625831

Weismüller, C., Urai, J.L., Kettermann, M., von Hagke, C. and Reicherter, K. 2019. Structure of massively dilatant faults in Iceland: lessons learned from high-resolution unmanned aerial vehicle data. *Solid Earth*, **10**, 1757–1784, https://doi.org/10.5194/se-10-1757-2019

Wheeler, J., Park, R.G., Rollinson, H.R. and Beach, A. 2010. The Lewisian Complex: insights into deep crustal evolution. *Geological Society, London, Special Publications*, **335**, 51–79, https://doi.org/10.1144/SP335.4

Whitehouse, M.J. 1989. Sm–Nd evidence for diachronous crustal accretion in the Lewisian Complex of Northwest Scotland. *Tectonophysics*, **161**, 245–256, https://doi.org/10.1016/0040-1951(89)90157-1

Whitehouse, M.J. and Kemp, A.I.S. 2010. On the difficulty of assigning crustal residence, magmatic protolith and metamorphic and ages to Lewisian granulites – constraints from combined *in situ* U–Pb and Lu–Hf. *Geological*

*Society, London, Special Publications*, **335**, 81–101, https://doi.org/10.1144/SP335.5

Whitehouse, M.J., Kemp, A.I.S. and Petersson, A. 2022. Persistent mildly suprachondritic initial Hf in the Lewisian Complex, NW Scotland: implications for Neoarchean crust–mantle differentiation. *Chemical Geology*, **606**, 121001, https://doi.org/10.1016/j.chemgeo.2022.121001

Wilson, R., Holdsworth, R.E. and Wightmand, R. 2011. Transect through the Canisp Shear Zone, Achmelvich, North-west Highlands – an excursion. Excursion 2. *In*: Goodenough, K.M. and Krabbendam, M. (eds) *A Geological Excursion Guide to the North-West Highlands of Scotland*. Edinburgh Geological Society, Edinburgh, 53–61.

Woodcock, N.H. and Mort, K. 2008. Classification of fault breccias and related fault rocks. *Geological Magazine*, **145**, 435–440, https://doi.org/10.1017/S0016756808004883

Zhu, X.K., O'Nions, R.K., Belshaw, N.S. and Gibb, A.J. 1997. Lewisian crustal history from *in situ* SIMS mineral chronometry and related metamorphic textures. *Chemical Geology*, **136**, 205–218, https://doi.org/10.1016/S0009-2541(96)00143-X